



Comparative study of five commonly used gravity type fish cages under pure current conditions

Hui Cheng, Lin Li, Muk Chen Ong*

Department of Mechanical and Structural Engineering and Materials Science, University of Stavanger, 4036, Stavanger, Norway

ARTICLE INFO

Keywords:

UiS-aqua
Gravity type fish cage
Numerical simulation
Cultivation volume
Cage deformation
Drag force

ABSTRACT

Gravity type fish cages have been commonly used in marine aquaculture for years. However, only limited research efforts have been made to assess the influences of different design parameters on the structural responses of gravity type fish cages. The present study first develops and validates an open-source numerical library under the toolbox Code_Aster for the structural analyses of fish cages. Then, the newly developed library is employed to conduct time-domain simulations to investigate the effects of the main design parameters on the cultivation volumes and drag forces. In this paper, five circumferences of the floating collar, five depths of the net bag, five weights and nine current velocities are considered in the parametric study of five commonly used fish cages. Moreover, regression functions are proposed based on the large number of numerical results to provide accurate predictions for the most concerning aspects in the design process for fish cages. Based on the parametric study, recommendations for selecting fish cage types and practical guides for cage construction are given. This study should be of value to structural designers as well as researchers wishing to optimise cage design.

1. Introduction

Aquaculture is a fast-growing industry. Over the past decades, the aquaculture industry has evolved from having a relatively minor role to playing a mainstream part in the global food system (Naylor et al., 2000, 2021). Fig. 1 presents the world aquaculture production from 1998 to 2018. The farmed finfish production, including inland, marine and coastal aquaculture, was 54.3 million tonnes and accounted for 47.4% of the global aquaculture production in 2018 (FAO, 2020b). Aiming for achieving a carbon-neutral goal, aquaculture is a promising direction for providing high-quality protein within a low carbon footprint. However, fish consumption only accounted for 17% of the total animal protein world widely, and this percentage is much lower in Oceania, Northern America and Europe (FAO et al., 2020). There is tremendous potential for aquaculture to raise dietary diversity in these areas. The fish meats require less land and freshwater for producing than any other animal meats (Froehlich et al., 2018). Moreover, finfish aquaculture creates fewer greenhouse gas emissions compared to land-based animal agriculture (Davis et al., 2016; Schubel and Thompson, 2019). Thus, as a substitute for land-based animal meats, fish meat should be promoted in daily life to meet the carbon-neutral goal. Currently, most of the finfish are produced from inland aquaculture (FAO, 2020a). However, the

expansion of this land-based aquaculture can negatively affect fresh water, soil, climate and biodiversity (Costello et al., 2020). This can compromise the ability of the inland environment to produce other food products. While covering 71% of Earth's surface, the ocean contributes only 13% to the world's farmed fish (FAO, 2020b). As the ocean has abundant high-quality water and virtually unlimited space, marine aquaculture has enormous potential for the supply of nutritious food in the future.

Fish cages are commonly used facilities in aquaculture. More than 150 fish species and 12 species of prawn, lobster and crab have been grown in cages (Beveridge, 2004). Over the past six decades, enormous types of fish cages have been proposed and developed (Chu et al., 2020; Guo et al., 2020; Huguenin, 1997; Xu and Qin, 2020; Sievers et al., 2021; Shainee et al., 2013a). However, the number of cage types today is smaller than it was two decades ago (Beveridge, 2004). Capital cost, which always comes at first, has become the overriding design criterion for industrial-scale fish farming, and this has led to an optimised design of cages by considering shape, size, and material). The gravity type fish cage, using High Density Polyethylene (HDPE) pipes as the skeleton to provide frame and buoyancy and using weight to keep cultivation volume, is now the first choice for most marine aquaculture sites. Since they are relatively inexpensive and convenient to build, this type of fish cage has been the dominant production technology for marine finfish

* Corresponding author. Department of Mechanical and Structural Engineering and Materials Science, University of Stavanger, 4036, Stavanger, Norway.
E-mail address: muk.c.ong@uis.no (M.C. Ong).

Nomenclature		λ	mesh grouping factor
A_t	outline area of a net panel	θ	inflow angle, where $\theta = 0^\circ$ indicates that the flow is aligned with the normal direction of a net panel
A_{net}	total area of netting in a fish cage	H	depth of net bag
C_D	drag force coefficient of a net panel	C	circumference of floating collar
C_L	lift force coefficient of a net panel	W	design weight (kg/m)
d_{wo}	physical twine diameter	W_0	total submerged weight (N)
E	Young's modulus	V_0	cultivation volume in still water
e_n	unit normal vector of a net panel	V	cultivation volume
L	half mesh size of net	D	diameter of floating collar
Sn	solidity of net	r	flow reduction factor
U	undisturbed incoming flow velocity	V_r	remaining volume factor

aquaculture in many counties, such as Norway, China, Japan, Chile, and Australia. For the countries with a low level of industrialisation, this cage technology has enormous potential for expansion, especially in inland and coastal waters (Cardia and Lovatelli, 2015; Edwards, 2015; Shainee et al., 2013b).

One of the main challenges for the gravity type fish cage is to ensure a sufficient cultivation volume for fish welfare. As the netting of a fish cage is usually flexible and may have large deformations under environmental loads, the cultivation volume can significantly decrease under severe currents and waves (Johannesen et al., 2021). In order to investigate the deformation and cultivation volume of fish cages, considerable research works have been done using experimental and numerical methods. Lader and Enerhaug (2005) measured the forces and geometry of a fish cage under the action of uniform flow in a flume tank. Lader et al. (2007a, 2007b) investigated the wave forces acting on and damping mechanism of a fish cage. Bi et al. (2015) conducted a series of laboratory experiments to investigate the damping effect of the net cage on wave propagation. Zhao et al. (2015a) investigated the hydrodynamic characteristics of a large fish farm containing eight cages with a model scale of 1:40. Their results showed that obvious flow-velocity reduction exists inside the cages of the multi-cage configuration. Dong et al. (2021) measured the drag force, cage deformation and flow field inside and around a scaled net cage model in a flume tank. Their results showed a complex fluid-structure interaction owing to the significant deformation of the flexible net. Bi et al. (2020) conducted laboratory experiments to investigate the effects of farmed fish on the drag force acting on fish cages. Their results suggested that the farmed fish has a negligible contribution to the drag force acting on

the cage. All of these experimental studies provide considerable and reliable results to understand the structural responses of fish cages.

While the experimental research offers down-scaled, controllable and repeatable conditions for reliable analysis (Buck and Langan, 2017), the complex dynamic behaviour of a full-scale fish cage is still largely uncertain from quantitative and sometimes qualitative points of view (Klebert et al., 2013; Ruzzo et al., 2021). The hydrodynamic responses of a gravity type fish cage mainly depend on gravity (buoyancy), elastic and viscous phenomena, which cannot be scaled using any scaling laws. In order to investigate the structural responses of full-scale fish cages, several in-house numerical codes have been developed in recent years and validated against experiments, and a few of these in-house codes turned into commercial software afterwards. Tsukrov et al. (2003) developed the Aqua-FE computer program (the latest version of the software is called Hydro-FE) and successfully applied it to the dynamic analysis of fish cage and mussel longlines (DeCew et al., 2010; Knysht et al., 2020, 2021). Through years of developments by Berstad et al. (2014, 2013, 2008) at Aquastructures AS, AquaSim became the leading analysis tool in the aquaculture industry in Norway. Li et al. (2006a, 2006b) and Zhao et al. (2007a, 2007b, 2007c) developed the DUT-FlexSim program with considerable validation works to calibrate their numerical models. Zhao et al. (2015b) compared the above two programs (Aqua-FE and DUT-FlexSim) with available experimental measurements and concluded that both programs have sufficient accuracy for the design of fish cages. With the contributions of considerable researchers worked at SINTEF Ocean (Endresen et al., 2014; Reite et al., 2014; Skjong et al., 2021; Su et al., 2019, 2021; Endresen and Klebert, 2020), the FhSim program was successfully developed with good

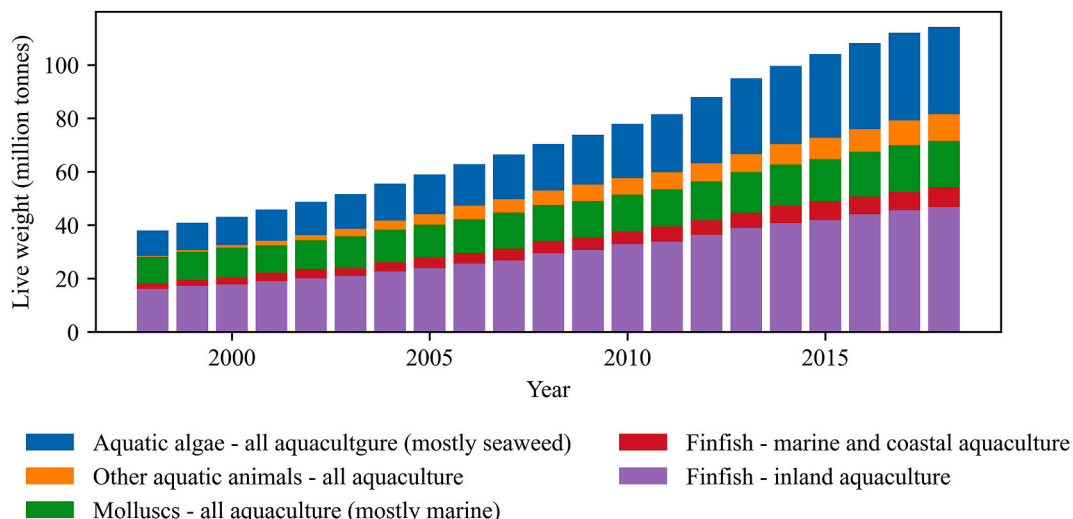


Fig. 1. World aquaculture production (FAO, 2020b).

verification and applied to various applications, such as fish cage in rough seas, trawl net system, aquaculture operation and structures in an ice floe. Lee (2002) and Cha and Lee (2002) developed a numerical tool and latterly applied it to fish cage analysis (Lee et al., 2008, 2015; Park et al., 2021). This numerical tool turned into commercial software, SimuTrawl, SimuPurse and SimuLine afterwards. Takagi et al. (2002) developed a numerical tool, NaLA, using similar numerical models as MPSTL, and applied it to estimate the dynamic responses of gill net, purse seine and fish cage (Suzuki et al., 2003; Shimizu et al., 2007; Takagi et al., 2014). Moreover, a handful of in-house codes also showed their ability to simulate the structural responses of fish cages (Wan et al., 2020; Wang et al., 2016; Huang et al., 2007; Priour, 2013; Chen et al., 2021; Kristiansen, 2013). A summary of the above codes, together with their adopted models, is shown in Table 1. A review of these hydrodynamic models employed by the above codes can be found in the research work by Cheng et al. (2020b).

Although considerable numerical solutions have been proposed with a large number of publications, most of these published numerical solutions are either commercial or still in-house. To the authors' knowledge, most of the codes listed in Table 1 cannot be accessed by the public without permission. In order to meet the high demand for a ready-for-use program, this paper develops a hydrodynamic library for an open-source program, CodeAster. This library, namely UisAqua, is stored in this repository (<https://github.com/hui-aqua/HydroModules>), together with a handful of examples and documents. Moreover, there is a need for the aquaculture industry to evolve from experienced-based design to knowledge-based design by verified numerical simulations, especially when the modern fish farm is growing up in developing countries. This paper investigates the structural responses of different cage designs and provides practical guides for cage constructions in the future.

In the present study, the detailed descriptions of the fish cages and the modelling method are presented in Sections 2 and 3. Section 4 comprehensively investigate the effects of the main design parameters on the cultivation volumes and drag forces by parametric study. Finally, the results are summarised with concluding remarks in Section 5.

2. Descriptions of the fish cage models

2.1. The main features of gravity type fish cages

As illustrated in Fig. 2, a typical fish cage usually comprises three main components (from top to bottom): floating collar, net bag, and weights. These three components determine the features of a fish cage. In addition, top net (for submersible cage or to prevent predation of birds), jumping net (to prevent fish jumping out of the cage) and skirt net (to reduce infestation of salmon lice) may be installed depending on the site conditions.

The floating collar, usually sitting at the water level, provides buoyancy force to sustain the cage floating, helps to maintain the net bag shape, serves as a work platform for operators, and offers handles to mooring lines for keeping the cage's position (Lekang, 2019). The

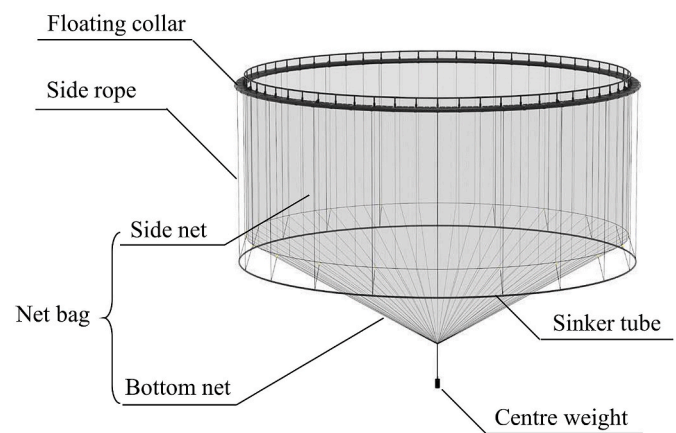


Fig. 2. Illustration of a typical gravity type fish cage (reproduced from AKVA Group (2020)).

structural design of the floating collar varies according to the available material, site condition and cage size. With years of development, the commonly used material for the floating collar is HDPE now due to its durability in sunlight and relatively low price.

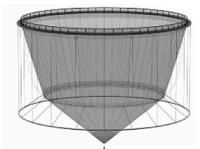
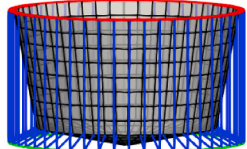
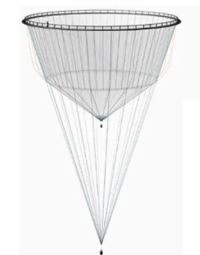
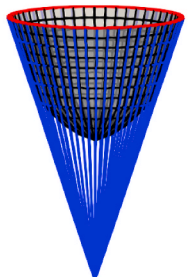
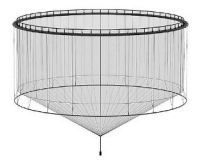
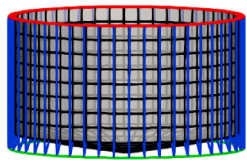

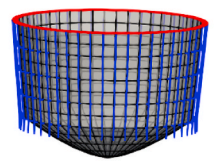

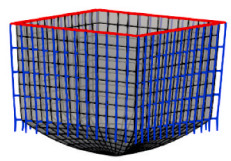
The weight, usually located at the bottom of a fish cage, is used to keep the net bag down and maintain as much effective volume as possible for the farmed fish (Lekang, 2019). In general, different forms of weight can be applied to a fish cage, such as (1) multiple-sinker weight (multiple sinkers attached to floating collars using side ropes), (2) single-sinker weight (only one single weight attached to the bottom net) and (3) sinker tube (one continuous pipe attached to the bottom net). Strong currents will decrease the cultivation volume, and increasing weights can suppress this. However, care must be taken because adding weights will increase the current forces on the net bag and increase the dynamic forces on the net bag caused by the waves (stretch and slack). The performance of these three forms of weight in steady current will be discussed in this study.

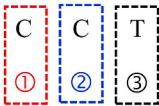
The net bag is regarded as the most critical part of a fish cage as it is the only barrier that protects the site environment from fish escapes. However, the netting should only keep the fish confined inside the net bag and should not have any structural functions, such as bearing loads and supporting cage shape (Cardia and Lovatelli, 2015). Nowadays, synthetic materials, e.g., Polyamide (PA, or nylon) and Polyethylene (PE), predominate in the aquaculture industry, because they are relatively cheap, strong and flexible (Lekang, 2019). The rope, acting as the skeleton of the netting, is usually the main structural component to ensure the strength and robustness of the net bag. All the weights of a cage are borne by the ropes and usually carried by the floating collar, in order to avoid the tearing damage on netting.

Table 1
Summary of codes for aquaculture structures.

Code	Available hydrodynamic model	Available structural model	Website
Hydro-FE (Aqua-FE)	Morison Model	Truss, beam, plate	–
AquaSim	Morison Model, Screen model	Truss, beam, membrane	https://aquasim.no/
DUT-FlexSim	Morison Model	Mass-spring	–
FhSim	Morison Model, Screen model	Truss, beam, membrane	https://fhsim.no/
SimuTrawl, SimuPurse, SimuLine	Morison Model	Mass-spring	http://www.mpsl.co.kr/
NaLA	Morison Model	Mass-spring	–

Table 2
A summary of the main characteristics of the studied fish cages.

Cage name ¹	Illustration ²	Numerical model ³	Description
CCT			CCT model is a truncated-cone shape cage with a double-pipe circular floating collar to provide buoyancy force and a sinker tube to weight down the net.
CCS			CCS model is a truncated-cone shape cage with a double-pipe circular floating collar to provide buoyancy force and a single-sinker weight to weight down the net.
CST			CST model is a straight shape cage with a double-pipe circular floating collar to provide buoyancy force and a sinker tube to weight down the net.
CSM			CSM model is a straight shape cage with a double-pipe circular floating collar to provide buoyancy force and multiple sinkers to weight down the net.
SSM			SSM model is a straight shape cage with a double-pipe square floating collar to provide buoyancy force and multiple sinkers to weight down the net.

1: Cage name	①	②	③
	The shape of floating collar	The shape of net bag	The form of weight
	C: Circular shape S: Square shape	C: Truncated-cone shape S: Straight shape	T: Sinker tube S: Single-sinker weight M: Multiple-sinker weight

2: The illustrations are gathered from a user manual created by AKVA Group (2020).

3: In the numerical model, the coloured components refer to the floating collar (red), ropes (blue), nettings (grey) and sinker tube (green).

2.2. Main parameters and environmental conditions

In the present study, five widely used gravity fish cages are modelled using the well-validated program by Cheng et al. (2020b). Table 2 summarise the main characteristics of these five fish cages, and the three-letter cage names reflect the characteristics of the three

components from top to bottom. The illustrations of these fish cages are reproduced from (AKVA Group, 2020). The common properties of the main components that are shared with all the fish cage models are listed in Table 3. These properties come from operating farms in the industry and have been applied in previous studies (Cheng et al., 2021; Endresen et al., 2014).

Table 3
The common properties of the main components for all the fish cage models.

Component	Parameter	Value	Unit
Netting	Twine diameter	2.85	mm
	Mesh length	25.87	mm
	Density	1140	kg/m ³
	Young's modulus	2	GPa
	Solidity	0.2056	–
	Mesh shape	Square	–
Sinker Tube	Section diameter	0.35	m
	Pipe thickness	0.0185	m
	Density	958	kg/m ³
	Young's modulus	3	GPa
Rope	Section diameter	50	mm
	Density	1100	kg/m ³
	Young's modulus	1	GPa
	Horizontal interval	2.5	m

Table 4
Summary of the studied parameters.

Parameter	Variable	Value	Unit
Circumference of floating collar	<i>C</i>	100, 120, 140, 160, 180	m
Depth of net bag	<i>H</i>	10, 20, 30, 40, 50	m
Weight ^a	<i>W</i>	40, 50, 60, 70, 80	kg/m
Current velocity	<i>U</i>	0, 0.1, 0.2, 0.3, 0.4, 0.5, 0.6, 0.7, 0.8	m/s

^a Weight: In the present study, the weight refers to the submerged weight per meter of circumference (Cardia and Lovatelli, 2015). E.g., for a fish cage with $W = 40$ kg/m and $C = 120$ m, the total submerged weight $W_0 = 40 \times 120 \times 9.81 = 47\,088$ N.

Moreover, in order to investigate the effects of the design parameters on the cultivation volumes and drag forces, 5 circumferences of floating collar (*C*), 5 depths of net bag (*H*), 5 design submerged weight (*W*) and 9 current velocities (*U*) are considered in the parametric study. Together with the 5 types of fish cages, there are $5 \times 5 \times 5 \times 9 \times 5 = 5\,625$ cases

in total. A summary of the studied parameters is shown in Table 4. Fig. 3 shows the studied parameters *H* and *C* in comparison with the previous studies (Bi and Xu, 2018; Cha and Lee, 2018; Cheng et al., 2018; Cheng et al., 2020a; Dong et al., 2021; Endresen and Klebert, 2020; Gansel et al., 2018; Huang et al. 2007, 2020; Lee et al., 2010; Winthereig-Rasmussen et al. 2016; Zhao et al., 2015a). In addition, three newly designed offshore fish cages, i.e., Deep Blue No.1, Ocean Farm 1 and Havfarm 1, are also shown in this figure for reference. It can be observed that all the studied fish cages satisfy $\frac{H}{C} \leq \frac{1}{2}$, which is the rule of thumb for the design of a gravity type fish cage (Cardia and Lovatelli, 2015).

According to the report by Halwart et al. (2007), most of the gravity type fish farms are located at sheltered sites. In the well-protected sea and freshwater sites, the wave force only accounts for a negligible fraction of environmental loads (Lekang, 2019). Thus, wave-induced forces are not included in this study. The maximum current velocity for simulations is set considering biological and environmental aspects. The strong current can wash away a large part of the feed causing unacceptable losses, and force farmed fish to swim causing worthless metabolic expenditure (Nilsen, 2019). For most of the finfish aquaculture, 0.2–0.5 m/s is the optimal current velocity, and 0.75 m/s is the maximum recommended current velocity (Cardia and Lovatelli, 2015). Thus, the current velocity in the present study is set from 0 m/s to 0.8 m/s with a 0.1 m/s interval.

3. Numerical method

3.1. Structural model

3.1.1. Governing equations

In the present study, a well-validated program, Code_Aster, is employed as the structural solver to calculate the structural responses of fish cages. The fish cage netting and ropes are divided into a set of line-type elements for calculating the structural responses. The equation governing the motions of Lagrangian nodes in the Cartesian coordinate system is:

$$[M]\ddot{q} + [K]q = F_g + F_b + F_h \tag{1}$$

where *q* is the time-dependent vector of nodal displacements, *M* is the

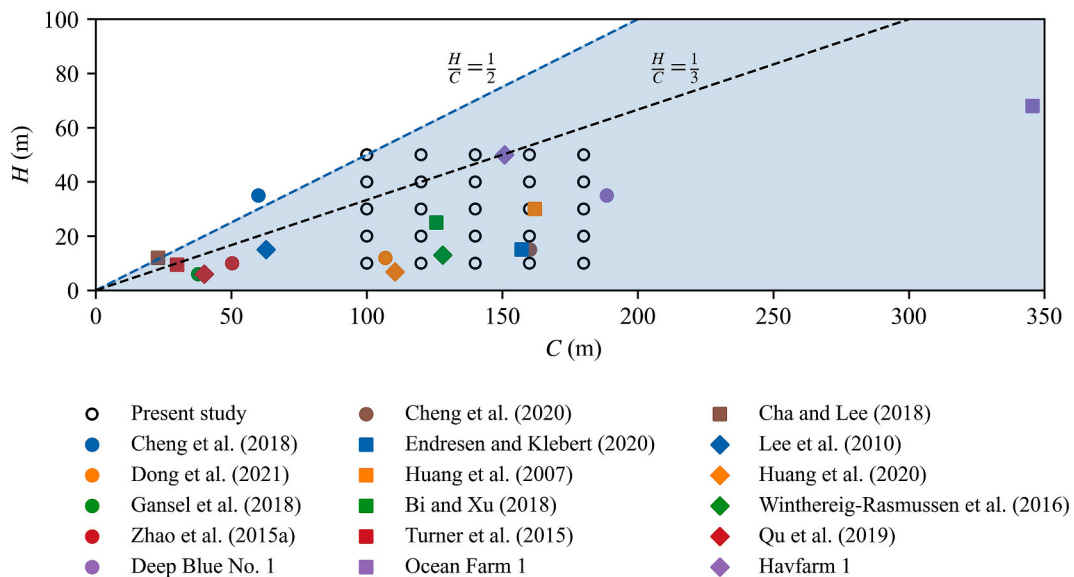


Fig. 3. The values of circumference and depth for net bags in the present and previous studies.

mass matrix, \mathbf{K} is the stiffness matrix, \mathbf{F}_g is the nodal force vector due to gravity, \mathbf{F}_b is the nodal force vector due to buoyancy, and \mathbf{F}_h is the nodal force vector for the hydrodynamic forces. Environmental loads on submerged nettings are on the right of Eq. (1). \mathbf{F}_h is calculated by the hydrodynamic force model. \mathbf{F}_g and \mathbf{F}_b are simple and only calculated once in the initialisation step, and they are constant throughout numerical simulations.

The system is highly nonlinear because the last term (\mathbf{F}_h) on the right-hand side depends on the time, the square of nodal velocities, and the structural deformations. According to Antonutti *et al.* (2018), the system nonlinearity can cause high-frequency oscillations and bring challenges for the simulations to reach convergence. In the present structural solver, the solution technique for Eq. (1) is based on the unconditionally stable Hilber-Hughes-Taylor- α (HHT- α) method with a variable time step, which introduces low numerical damping in the low-frequency band and high damping at the high-frequency band.

3.1.2. Finite element constitution

Two types of structural elements, *i.e.*, bar and beam, are used in the present study to model the fish cage. The bar element is employed to model the fully flexible components, such as ropes and the twines in netting. This element is denoted as ‘‘CABLE’’ in the structural solver and follow the three assumptions in the present simulations:

1. The material is linearly elastic.
2. The strains in cable elements are small, but displacements are large (geometric nonlinearity).
3. Loading is applied at nodes.

In practice, a mesh grouping method is usually adopted in the modelling of netting to reduce the computational effort. In order to achieve equivalent numerical results, the derived diameters d_{ws} and d_{we} are applied during the model building. The detailed derivation and explanation can be referred to Cheng *et al.* (2020b). Here, only the relationships between the derived diameters and the physical twine diameter (d_{w0}) for nettings with square meshes are presented:

$$d_{ws} \approx \sqrt{\lambda}d_{w0}; \quad d_{we} = \sqrt{\lambda}d_{w0}; \quad (2)$$

where λ is the mesh grouping factor which is defined as the ratio between the mesh sizes of the numerical netting and the physical netting.

The beam element is employed to model the sinker tube and the

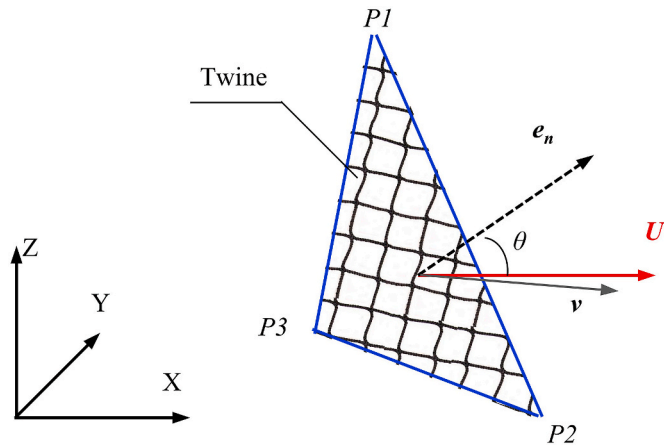


Fig. 4. Illustration of the Screen model. The inflow angle θ of the net-panel is the angle between \mathbf{e}_n and \mathbf{U} .

floating collar, which can take bending and torsional loads. This element is denoted as ‘‘POU_D_E’’ in the structural solver and using the Euler–Bernoulli beam theory.

3.2. Hydrodynamic model

As the hydrodynamic forces on the fish cage are complex, a hydrodynamic force model is required to calculate the forces on structures and transfer the forces to the structural solver. In the present study, a hybrid hydrodynamic model is applied to calculate the environmental loads on the different components of the fish cage. For the netting, a membrane-like structure, the Screen model originally proposed by Kristiansen and Faltinsen (2012) is employed to calculate its hydrodynamic forces. For the rope, floating collar and sinker tube, the Morison model is employed to calculate its hydrodynamic forces.

3.2.1. Hydrodynamic model for netting

The hydrodynamic force on netting is related to many parameters, such as Reynolds number, solidity ratio, attack angle, knot type and twine construction (Tang *et al.*, 2018). However, fully resolving all these parameters is computational demanding for industrial usages. Thus, a Screen model, considering the main contributors of these related parameters, is proposed by Kristiansen and Faltinsen (2012) and now is widely used in numerical simulations. Fig. 4 illustrates the Screen model employed in the present study to calculate the hydrodynamic forces (\mathbf{F}_h) on netting. Screen models are theoretically superior to Morison models for calculating the force on nettings as the twine-to-twine interaction is implicitly included in the force calculation (Cheng *et al.*, 2020b). The hydrodynamic forces are decomposed into drag force F_D and lift force F_L , and the two components are calculated using Eqs. (3) and (4):

$$F_D = \frac{1}{2}C_D\rho_w A_t |U - \mathbf{v}|^2 i_D \quad (3)$$

$$F_L = \frac{1}{2}C_L\rho_w A_t |U - \mathbf{v}|^2 i_L \quad (4)$$

where ρ_w is the fluid density, A_t is the area of the net panel (the area of the triangular P1–P2–P3 in Fig. 4), \mathbf{U} is the velocity of the fluid at the centroid of the net panel, \mathbf{v} is the velocity of the structure. The unit vectors i_D and i_L which are used to indicate the directions of forces, and they are defined by Eqs. (5) and (6). C_D and C_L are the drag and lift force coefficients in the Screen model, respectively. These force coefficients in Eqs. 7–14 have been validated by many studies (Cheng *et al.*, 2020b; Kristiansen and Faltinsen, 2012).

$$i_D = \frac{\mathbf{U} - \mathbf{v}}{|\mathbf{U} - \mathbf{v}|} \quad (5)$$

$$i_L = \frac{(\mathbf{U} - \mathbf{v}) \times \mathbf{e}_n \times (\mathbf{U} - \mathbf{v})}{|(\mathbf{U} - \mathbf{v}) \times \mathbf{e}_n \times (\mathbf{U} - \mathbf{v})|} \quad (6)$$

$$C_D = C_{D0} (0.9\cos\theta + 0.1\cos3\theta) \quad (7)$$

$$C_L = C_{L0}(\sin2\theta + 0.1\sin4\theta) \quad (8)$$

$$C_{D0} = C_{cylinder} \frac{Sn(2 - Sn)}{2(1 - Sn)^2}; \quad (9)$$

$$C_{L0} = \frac{0.5C_{D0} - C_{L45}}{\sqrt{2}}; \quad (10)$$

$$C_{L45} = \frac{\pi C_{N45}}{8 + C_{N45}}; \quad (11)$$

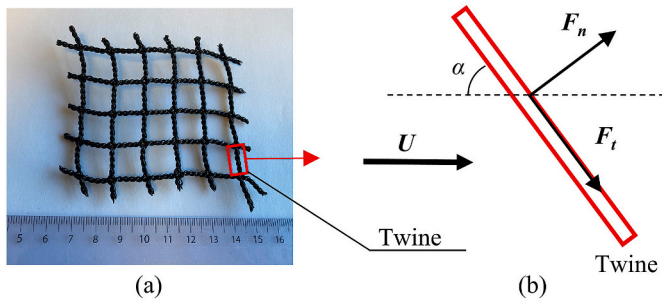


Fig. 5. A 2D illustration of the hydrodynamic forces on cable or pipes. F_n and F_t are the normal and tangential drag forces, respectively. The angle of attack α is the angle between the current direction and the axis of the rope or pipes.

$$C_{N45} = C_{cylinder} \frac{Sn}{2(1 - Sn)^2} \quad (12)$$

$$C_{cylinder} = 78.46675 + 254.73873 \log_{10} Re - 327.8864 (\log_{10} Re)^2 - 223.64577 (\log_{10} Re)^3 - 87.92234 (\log_{10} Re)^4 + 20.00769 (\log_{10} Re)^5 - 2.44894 (\log_{10} Re)^6 + 0.12479 (\log_{10} Re)^7 \quad (13)$$

$$Re = \frac{d_w(U - v)}{\nu(1 - Sn)} \quad (14)$$

3.2.2. Hydrodynamic model for ropes, floating collar and sinker tube

Fig. 5 illustrates the Morison model that is used in the present study to calculate the hydrodynamic forces (F_h) on the rope, floating collar and sinker tube. In the Morison model, the hydrodynamic forces are decomposed into two components: normal drag force (F_n , Eq. (15)) and tangential drag force (F_t , Eq. (16)):

$$F_n = \frac{1}{2} C_n \rho L d_w |u^n| u^n \quad (15)$$

$$F_t = \frac{1}{2} C_t \rho L d_w |u^t| u^t \quad (16)$$

where L is the length of an element, d_w is the section diameter, ρ is the fluid density. u^n and u^t are the normal and tangential velocity of fluid relative to the twine. C_n and C_t are the normal and tangential drag coefficients. The two force coefficients employed in this study are from DeCew et al. (2010), as described by Eqs. 17–20.

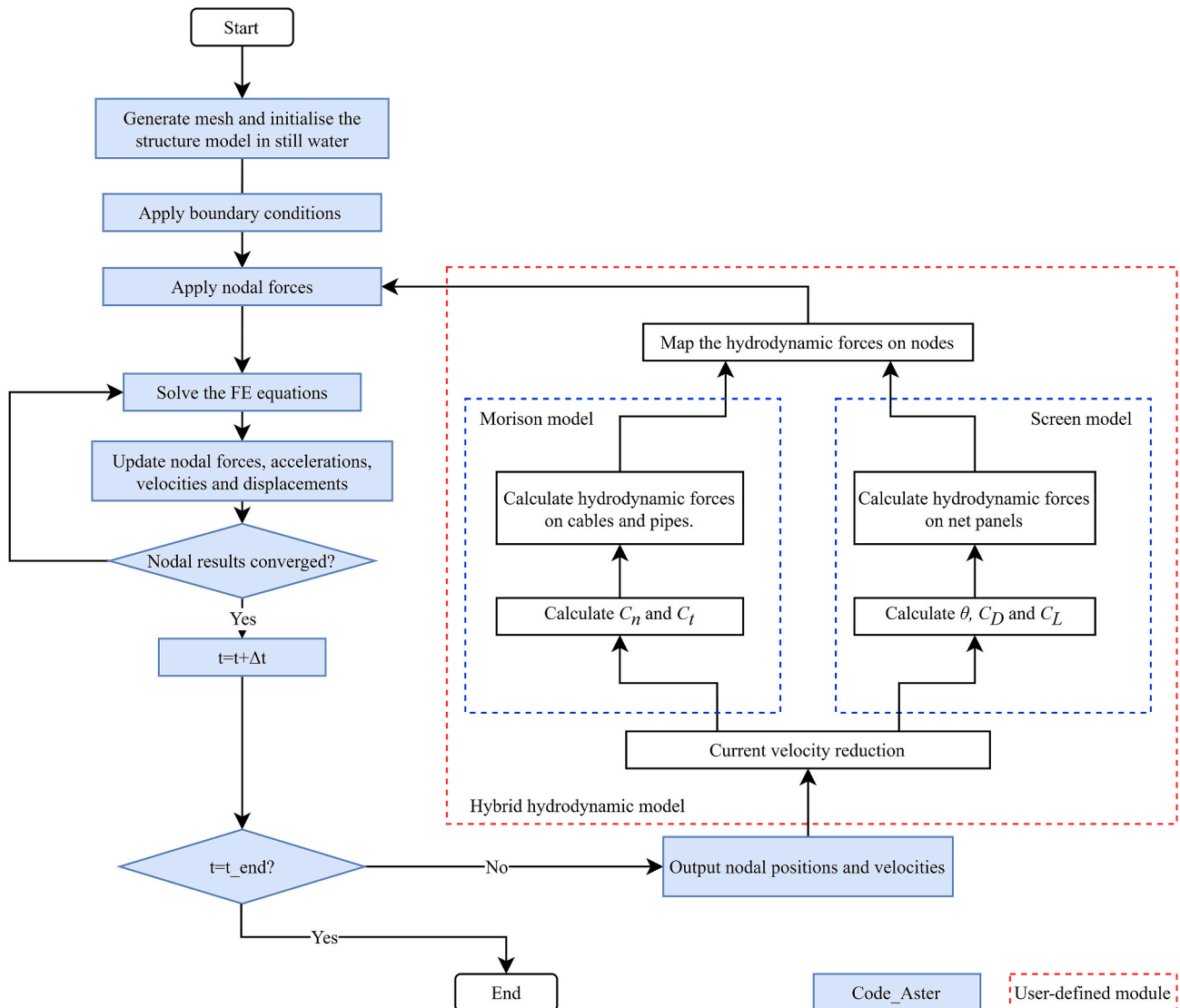


Fig. 6. Flowchart for the simulation process.

$$C_n = \begin{cases} \frac{8\pi}{sRe} (1 - 0.87s^{-2}) & 0 < Re < 1 \\ 1.45 + 8.55Re^{-0.9} & 1 < Re < 30 \\ 1.1 + 4Re^{-0.5} & 30 < Re < 2.33 \times 10^5 \\ -3.41 \times 10^{-6} (Re - 5.78 \times 10^5) & 2.33 \times 10^5 < Re < 4.92 \times 10^5 \\ 0.401 \left(1 - e^{\frac{-Re}{5.99 \times 10^5}}\right) & 4.92 \times 10^5 < Re < 10^7 \end{cases} \quad (17)$$

$$C_t = \pi\mu (0.55\sqrt{Re} + 0.084Re^{2/3}) \quad (18)$$

$$s = -0.077215665 + \ln(8 / Re); \quad (19)$$

$$Re = \frac{d_w(U - v)}{\nu} \quad (20)$$

3.2.3. Wake effects

When the current passes one net panel, the current velocity will be reduced by the friction from the twines in the net panel. This velocity-reduced current results in a smaller drag force on downstream net panels compared to upstream ones. In order to calculate the forces on downstream net panels, it is necessary to know how much the velocity is reduced, particularly since the velocity is squared in hydrodynamic models, so it gives a large contribution. In practice, a flow reduction factor (r) is adopted to represent this current velocity reduction, as expressed by Eq. (21).

In this study, the flow reduction factor, as expressed by Eq. (22), is employed to predict the velocity reduction. The formula in Eq. (22) is originally proposed by Cheng et al. (2020b) and is validated with experiments, showing high accuracy.

$$U_{downstream} = rU_{\infty} \quad (1 < r < 1) \quad (21)$$

$$r = f_2(Sn, \theta) = \max\left(0, \frac{\cos \theta + 0.05 - 0.38Sn}{\cos \theta + 0.05}\right) \quad (22)$$

The flowchart for the present simulation process is presented in Fig. 6. The hybrid hydrodynamic module, highlighted by the red dashed box in Fig. 6, is invoked at each time step to calculate the hydrodynamic

forces on the nets, ropes and pipes, and maps these hydrodynamic forces onto corresponding nodes. The two types of hydrodynamic models, i.e., Screen model and Morison model, are employed for the different components explained in Sections 3.2.1 and 3.2.2.

3.3. Validation of the numerical library

Validation simulations based on the experiments by Moe-Føre et al. (2016) have been conducted to verify the present numerical library in the previous work by Cheng et al. (2020b). Fig. 7 shows the drag forces and cage deformation using the present numerical library. According to Fig. 7(a), the maximum relative different between the present numerical results and the experimental results is only 5%. According to Fig. 7(b), the fish cage shape using the present numerical library agrees well with the experiments by Moe-Føre et al. (2016). For more detailed information about simulation setup can be found in the work by Cheng et al. (2020b).

3.4. Simulation process

In the present study, all the simulations are conducted in the time domain. The settings of time step and mesh size are based on the previous convergence studies by Cheng et al. (2020b). All the simulation cases adopt a mesh size of 2.5 m, a time step of 0.2 s and a simulation duration of 600 s. Fig. 8 shows the time series of numerical results for the five types of fish cages when $C = 120$ m, $H = 30$ m, $W = 40$ kg/m and $U = 0.3$ m/s. In order to reduce initial impact effects, the current velocity in the present study is linearly increased from 0 m/s to the targeted

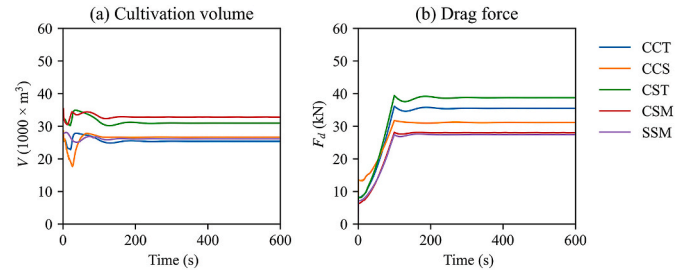


Fig. 8. Time histories of cultivation volumes and drag forces for the five gravity type fish cages with $C = 120$ m, $H = 30$ m, $W = 40$ kg/m and $U = 0.3$ m/s.

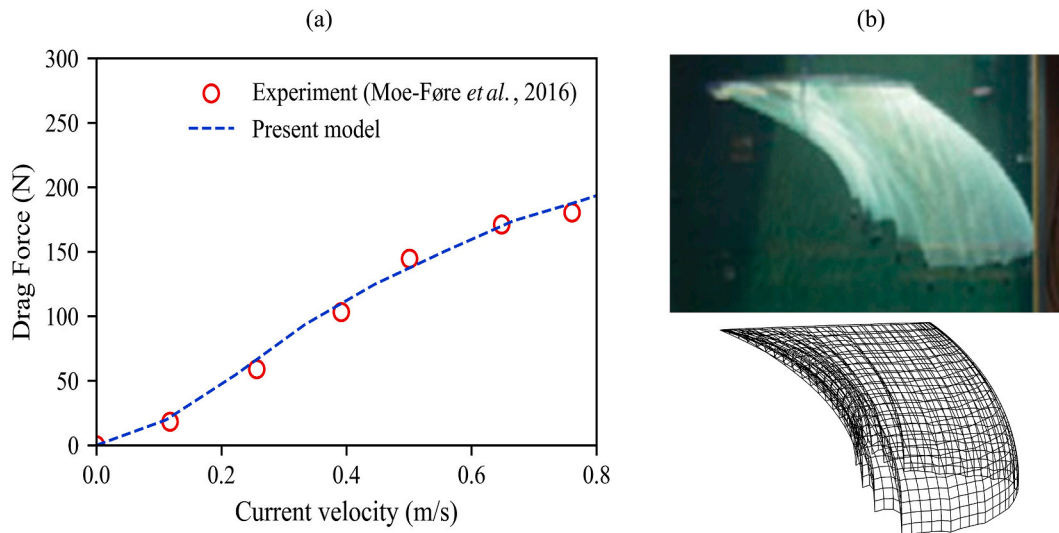


Fig. 7. Validation results of the present numerical library against experiment by Moe-Føre et al. (2016). (a) The drag force on the fish cage at different velocities. (b) The deformation of fish cage when the current velocity is 0.4 m/s.

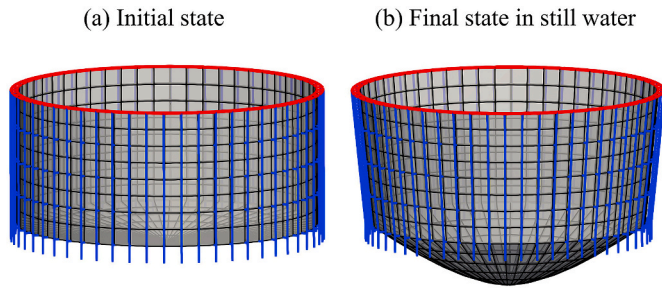


Fig. 9. The cage shape in still water.

velocity within the first 100 s. All the simulations can reach a steady state after 300 s. The mean value of the drag force and cultivation volume is measured from the last 300 s and will be used in the subsequent discussions.

Fig. 9 shows the shape of the CSM fish cage in still water. Compared to its initial geometrical configuration, the cage is deeper in the final state as the weight can stretch down the bottom net. Meanwhile, the side net moves towards the centre of the fish cage due to the lack of support from sinker tube. Thus, the cultivation volume in still water may be larger than its initial volume in structural analyses. The cultivation volume is calculated based on the divergence method, as described by Eq. (23). The remaining volume factor is defined as the ratio between the cultivation volume under various current velocities and its corresponding volume in still water: $V_r = \frac{V}{V_0}$.

$$V = \iiint_{\Delta} (\nabla \cdot f) dV = \iint_{\Delta} (f \cdot n) dA_s \quad (23)$$

4. Results and discussion

4.1. Cultivation volume in still water

4.1.1. Volume and total netting area in still water

Traditionally, the dimensions of a fish cage are empirically determined. In order to accurately estimate the cultivation volume in still water and the total netting area for commonly used gravity type fish cage, regression functions are proposed in the present study, as shown in Eqs. (24) and (25), where a_1, a_2 are the slopes and b_1, b_2 are the intercepts. For each regression function, the numerical results from $5 \times 5 = 125$ combinations of C, H and W are considered. The regression functions are shown in Fig. 10 together with the numerical results and their regression coefficients are listed in Table 5.

As shown in Fig. 10(a), the cultivation volume in still water V_0 can be well estimated by Eq. (24) using the design parameters C and H . The regression functions of SSM and CCS are almost overlapped coincidentally. The intercept b_1 in the formula for the volume prediction is related

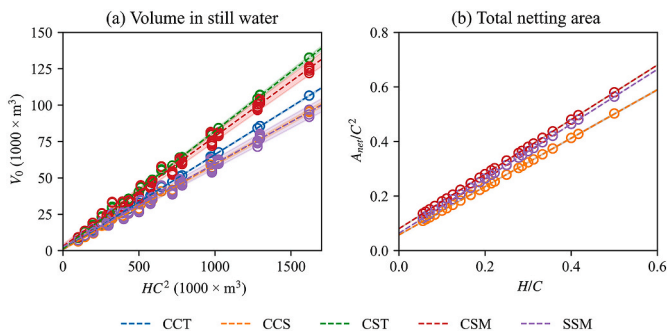


Fig. 10. Estimations of cultivation volume in still water and total netting area using C and H . The shadows show the 99.7% confidence intervals for the regression functions in Eqs. (24) and (25).

Table 5

Regression coefficients for Eqs. (24) and (25).

Cage name	Coefficients in Eq. (24)			Coefficients in Eq. (25)		
	a_1	b_1	R^2	a_2	b_2	R^2
CCT	0.0654 ± 0.0003	0.6192 ± 0.1938	0.9998	0.8868 ± 0.0023	0.0573 ± 0.0006	0.9999
CCS	0.0585 ± 0.0007	0.8032 ± 0.5035	0.9981	0.8868 ± 0.0023	0.0573 ± 0.0006	0.9999
CST	0.0811 ± 0.0006	1.0788 ± 0.4380	0.9992	1.0000 ± 0.0004	0.0801 ± 0.0001	1.0000
CSM	0.0755 ± 0.0020	2.9287 ± 1.4324	0.9908	1.0000 ± 0.0004	0.0801 ± 0.0001	1.0000
SSM	0.0573 ± 0.0019	2.4335 ± 1.3399	0.9851	1.0015 ± 0.0009	0.0632 ± 0.0002	1.0000

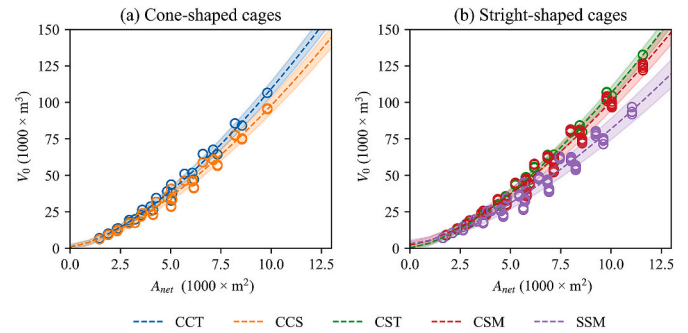


Fig. 11. Cultivation volumes of fish cages in still water with various dimensions. The shadows show the 99.7% confidence intervals for the regression function Eq. (26).

to the cone-shaped bottom. As the cone depth is only 3 m in this study, the intercept is negligible compared to the predicted V_0 . The total netting area of a fish cage (A_{net}) is only related to the shape of its net bag, as shown in Fig. 10(b). Eq. (25) can give high-accurate estimations for A_{net} . By using these two regression functions, the volume and netting can be easily quantified in the preliminary design process.

$$V_0 = a_1 HC^2 + b_1 \quad (24)$$

$$A_{net} = a_2 HC + b_2 C^2 \quad (25)$$

4.1.2. Effect of cage dimension on cost per unit volume

$$V_0 = a(A_{net})^{1.5} + b \quad (26)$$

In order to compare the cost per unit volume of the five types of fish cages in still water, the cultivation volume of the fish cages with varying dimensions and weights are shown in Fig. 11. Five fitted curves are plotted for the corresponding cage using the same colour. The form of the fitted curves is described by Eq. (26), and the regression coefficients (a and b) are listed in Table 6.

When the cages are in still water, increasing W cannot bring additional cultivation volume. Thus, W is not included in the regression function. According to Eq. (26), the speed of volume increment is faster

Table 6

Regression coefficients for Eq. (26).

Cage name	Coefficients		R^2
	a	b	
CCT	3.4252 ± 0.1099	0.9168 ± 1.5120	0.9861
CCS	3.0585 ± 0.1176	1.1463 ± 1.6172	0.9802
CST	3.3500 ± 0.0835	0.3051 ± 1.4832	0.9916
CSM	3.1107 ± 0.1262	2.3315 ± 2.2408	0.9780
SSM	2.4852 ± 0.1536	3.1715 ± 2.4125	0.9515

than the speed of netting area increment when the dimension of a cage is increased. Thus, the construction cost per unit volume of a fish cage is reduced with the increasing dimension. While large cages could improve profitability, they may increase the risk of low dissolved oxygen (DO) conditions due to reduced water exchange (Oldham et al., 2018). Thus, it needs to balance the risk and profitability during the design. Besides, the cost per unit volume of a fish cage also depends on other factors, such as net bag shape and forms of weight. The influences of these factors become significant when the fish cage has a large dimension, e.g., when $A_{net} > 10\,000\text{ m}^2$ or $V_0 > 100\,000\text{ m}^3$. When the cage becomes large, CCT and CST have the lowest cost per unit volume among the five studied types, as they can provide the largest cultivation volume with the same area of netting.

4.1.3. Effect of net bag shape on cost per unit volume

The net bag shape is mainly determined by the shape of the floating collar, the ratio of bottom circumference to top circumference and the ratio of cage depth to circumference (H/C). H/C can indicate how slim or stout a cage is. A large value of H/C means the cage is slim; otherwise, the cage is stout. According to the Norwegian Standards NS 9415 (Standards Norway, 2009) and Lekang (2019), H/C should not exceed 0.4 for straight circular cages, and 0.5 for cone-shape cages.

The shape of the floating collar can affect the efficiency of material usage. With the same length of the floating collar, the circular shape makes the most efficient use of materials and thus can provide a larger surface area and larger cultivation volume than the square shape. In addition, corners of square structures may be little utilised due to the circular swimming behaviours of fish (Beveridge, 2004), and these corners can be sharper under higher current velocities, as shown in Fig. 12(c).

The ratio of bottom circumference to top circumference determines how the cage is tapered. The tapered cages, which get narrow from the top down to the bottom, have similar shapes caused by the gravity. Taking CCT and CST as examples, the truncated-cone shape net bag may wisely use the nettings, as the side net usually moves towards the centre of a cage (Fig. 9(b)). In the present study, the ratio of bottom circumference to the circumference is 0.8 for the cone-shaped cages (CCT and CCS), which is similar to the cage employed by Endresen and Klebert (2020). This ratio can be optimised to improve the efficiency of material usage through further parametric study, but it is out of scope in the present work.

Fig. 13 shows how the H/C affects the cost per unit volume. For a given cultivation volume, the increment of H/C , which makes the cage stouter, can improve the efficiency of materials usages. Besides, this figure can also indicate that among the five cages, the SSM has the highest cost per unit volume for same H , C and W . For sites with small current velocity, it is suggested to enlarge the fish cage vertically, because when $H/C < 0.5$, 1 m increment of cage depth can gain more cultivation volume than 1 m increment of cage circumference. This can

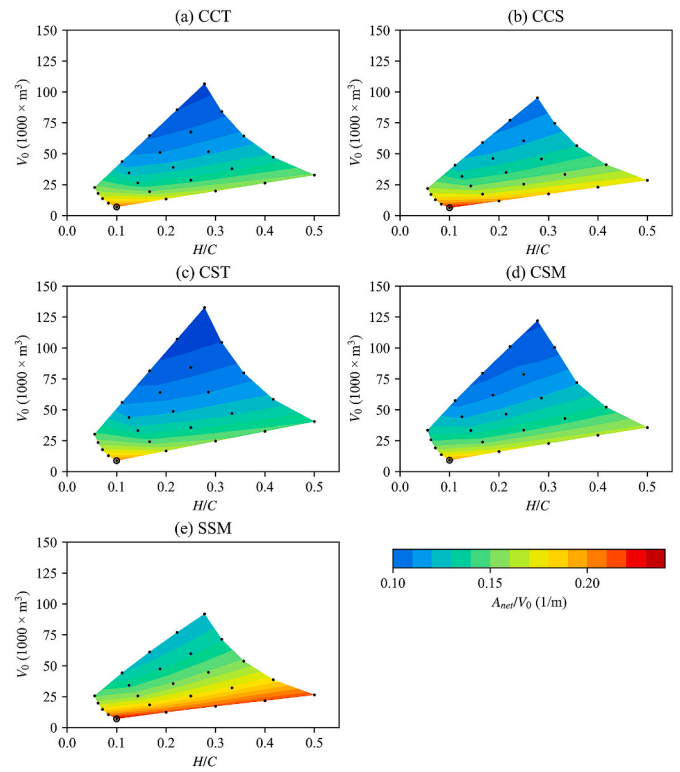


Fig. 13. Cultivation volumes in still water and netting area to volume ratio for fish cages with different H/C when $W = 40\text{ kg/m}$. The black points represent the studied cases. The black circles represent the case with $H = 10\text{ m}$ and $C = 100\text{ m}$.

be easily proved by assessing the partial derivatives of Eq. (24)

4.1.4. Effect of weight on cost per unit volume

Although increasing the weight cannot bring any additional cultivation volume in still water, the forms of weight can still affect the cultivation volume. As shown in Fig. 13, when CCT and CCS have the same dimensions, the CCT can gain roughly 10% larger volume than CCS, because its sinker tube can restrict the side net and prevent it from moving towards the cage centre, as shown in Fig. 9(b). In addition, the comparison between CST and CSM also indicates that the sinker tube can bring more volume to the cage than the multiple-sinker weight. Thus, it is suggested to adopt the sinker tube as the weight for the cage in still water or sites with low current velocities.

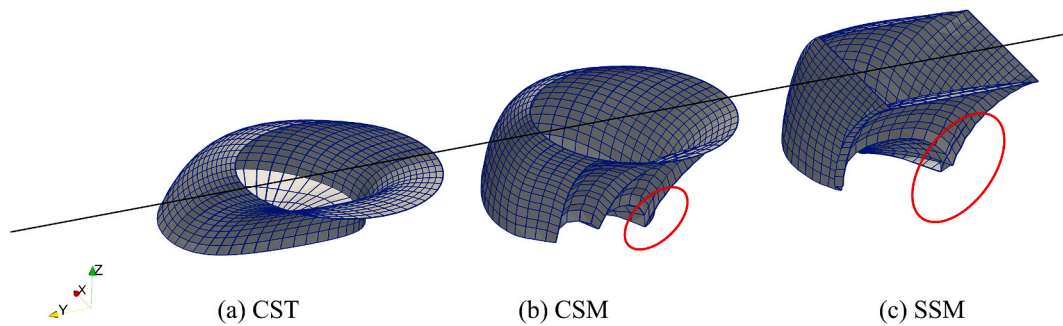


Fig. 12. The deformations of different net bags. Sharp coners (circled in red) appear in the net bags using multiple-sinker weight with $C = 120\text{ m}$, $H = 40\text{ m}$, $W = 50\text{ kg/m}$ and $U = 0.6\text{ m/s}$. These sharp coners may not be used by the farmed fish if the fish has circular swimming pattern. (For interpretation of the references to colour in this figure legend, the reader is referred to the Web version of this article.)

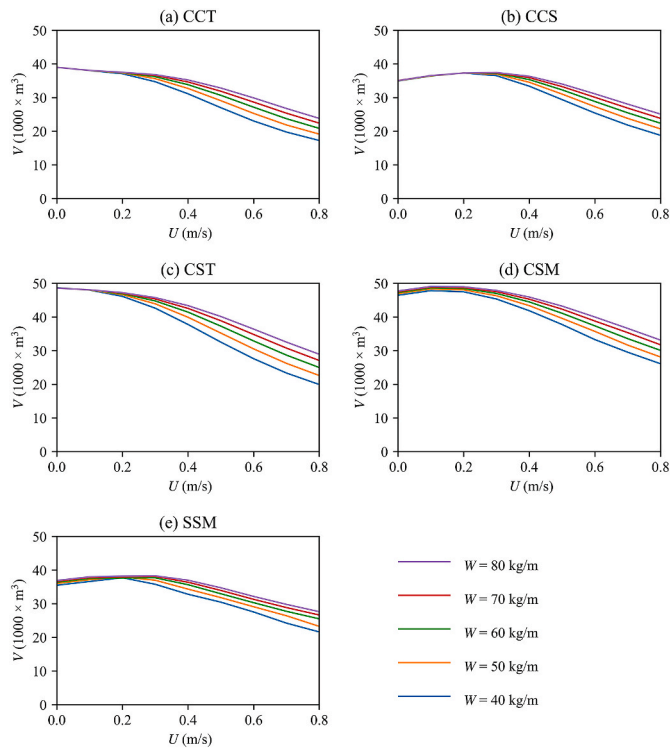


Fig. 14. Cultivation volumes of the five fish cages with $C = 140 \text{ m}$ and $H = 30 \text{ m}$ under different current velocities.

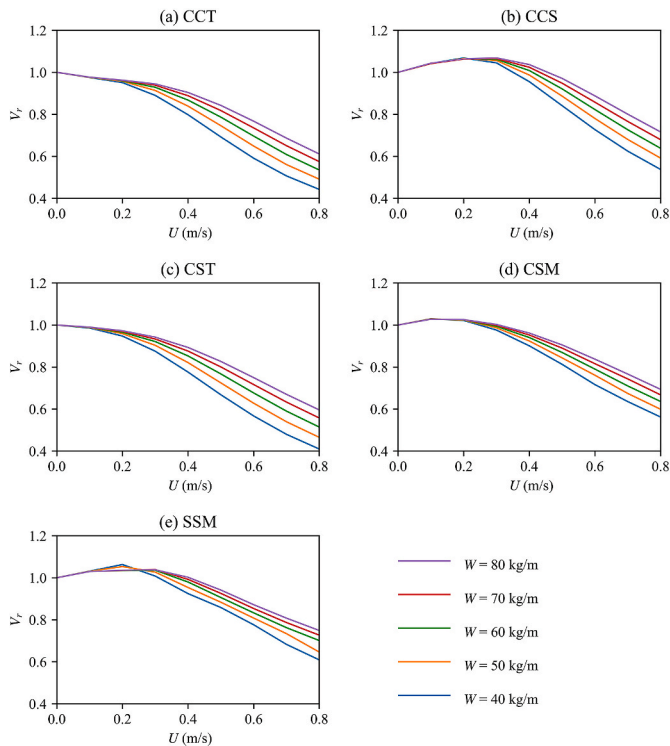


Fig. 15. Remaining volume factors for the five fish cages with $C = 140 \text{ m}$ and $H = 30 \text{ m}$ under different current velocities.

4.2. Cultivation volume under current conditions

4.2.1. Effect of current velocity on cultivation volume

Although cage culture can be carried out successfully even in still

water, a certain water current (0.1–0.2 m/s) has a good effect on the oxygen supply and the fish muscle development, ensuring permanent water exchange between the water body inside and outside of the cage (Cardia and Lovatelli, 2015). As the gravity type cages do not have rigid nets, strong current velocity can easily reduce the cultivation volume and cause negative impacts on fish welfare. Fig. 14 shows that the cultivation volumes of the five types of fish cage are reduced significantly with the increasing current velocity but increasing the weight can mitigate the volume reduction.

Fig. 15 shows V_r for the five types of fish cages under different U . The cultivation volume of a fish cage can reduce to half of its cultivation volume in still water when $U > 0.5 \text{ m/s}$. Cages using different forms of weight may have different abilities to keep cultivation volume. However, when $U < 0.2 \text{ m/s}$, values of V_r for the five types of cages are all close to 1. For the cages using sinkers as weight, i.e., CCS, CSM and SSM, V_r even increases slightly, up to 1.1, when $U < 0.2 \text{ m/s}$. This means the cultivation volumes of gravity type fish cages can be well maintained under such small current velocities. According to Halwart et al. (2007), with a current velocity of 0.15 m/s, the water in a fish cage can be exchanged more than 100 times per day, which already exceeds the typical amount needed to ensure the levels of nutrients in the water column. Thus, gravity type fish cages are suitable for sites with small current velocities.

4.2.2. Effect of weight system on cultivation volume

Faster current velocities usually require heavier weights. As shown in Figs. 13 and 14, the increment of W can mitigate the volume loss caused by strong currents. However, the cost-effectiveness of increasing weight depends on the form of weight and the current velocity in the site. When $U < 0.2 \text{ m/s}$, the increment of W may not bring obvious benefits to the cultivation volume, but can bring additional costs and burdens to weight-related operations. When $U > 0.2 \text{ m/s}$, the increment of weight helps to mitigate the fish cage deformation, but at the same time, reduces total buoyancy. Thus, the total weight of a gravity type fish cage should be well designed depending on the site's current velocity and the buoyancy. Besides, the forms of weight may also affect cage deformations.

Fig. 16 shows the deformations of the five net bags with different forms of weight. According to Cardia and Lovatelli (2015), although sinker tubes are more expensive than sinkers, the sinker tubes may better maintain the shape of the cage bag, as the sinker tubes have a certain stiffness. The top and front views in Fig. 16 also indicate that the bottom nets of the cages using sinker tube are flatter than those using single-sinker weight or multiple-sinker weight. However, the flatter bottom nets are not enough to guarantee a larger volume than those without flat bottoms. As shown in Fig. 16, CCS, CSM and SSM may not have a flat bottom, but they can have deeper cage bags. Thus, it is difficult to judge which forms of weight can produce the largest cultivation volume for the same design parameters.

4.2.2.1. Sinker tubes versus single-sinker weight (CCT vs. CCS). Based on the results in Fig. 15, the cage using single-sinker weight has a larger V_r than that using sinker tube when both have the same C , H , W and under the same U . Fig. 17 shows how these two forms of weight systems affect the cage deformations. As observed from this figure, the bottom net of CCT is flatter than that of CCS. This is because the tensional ropes between the sinker tube and bottom net can mitigate the vertical stretch of the bottom net. Thus, the bottom net of CCT is almost in the same plane as the sinker tube. The sinker tube can better maintain the shape of net bag compared to the single-sinker weight, but it may result in a smaller cultivation volume due to the flat bottom net. The nearly flat bottom net acts as a porous airfoil that can provide a lift force to raise the bottom net, thus reducing cultivation volume. Therefore, from the perspective of volume maintenance, the sinker tube is no better than the single-sinker weight, which is contrary to the observations by Cardia and

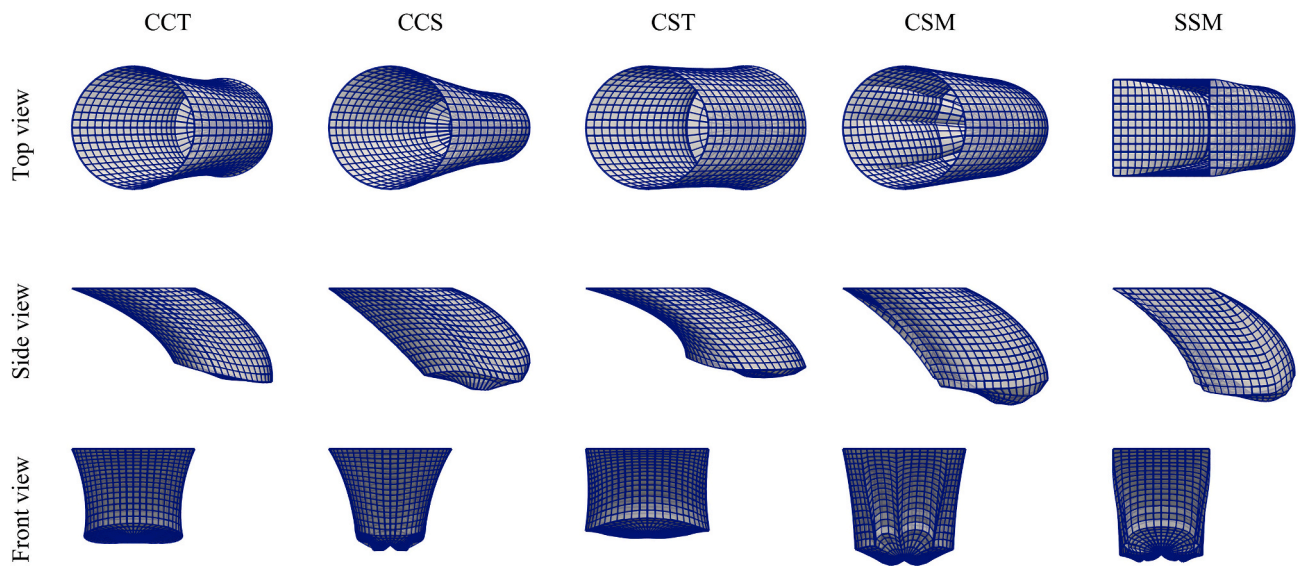


Fig. 16. Deformations of the five net bags with $C = 120$ m, $H = 40$ m, $W = 50$ kg/m and $U = 0.6$ m/s.

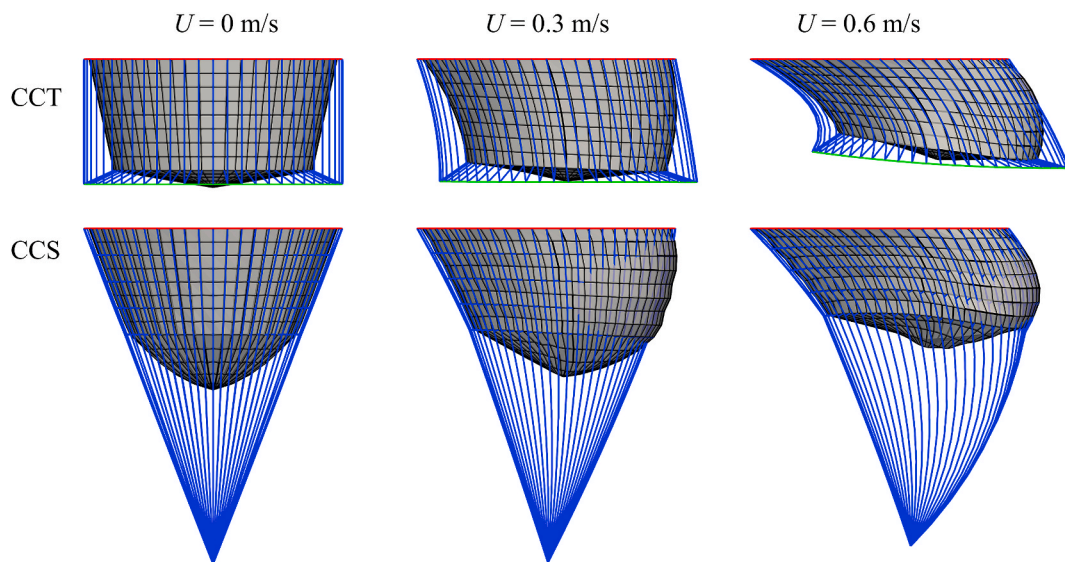


Fig. 17. Deformations of the two truncated-cone shape fish cages with $C = 140$ m, $H = 20$ m and $W = 50$ kg/m under three current velocities.

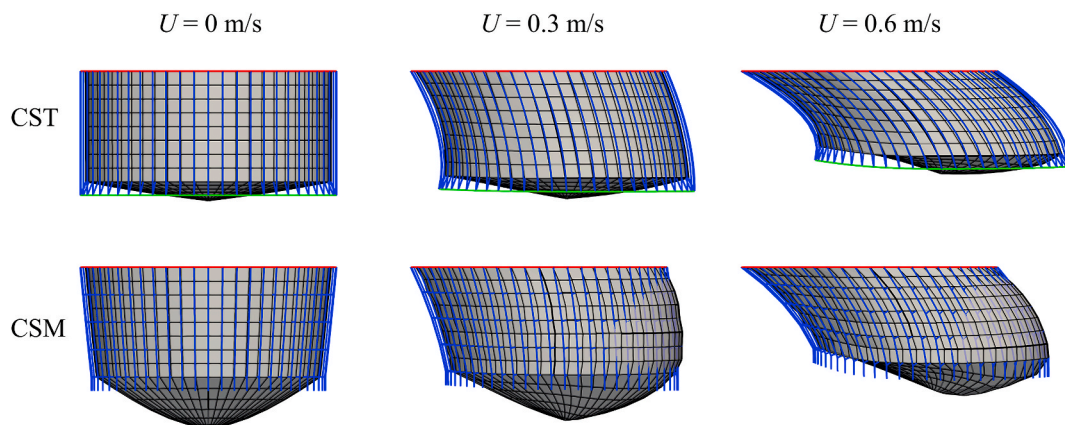


Fig. 18. Deformations of the two circular straight shape fish cages with $C = 140$ m, $H = 20$ m and $W = 50$ kg/m under three current velocities.

Lovatelli (2015). However, considering CCT has a larger initial volume in still water than the CCS when the two cages have the same dimension, the larger V_r of CCS may make the actual cultivation volumes of the two type cages roughly equal. Their similar cultivation volumes are evident in Fig. 14.

4.2.2.2. Sinker tubes versus multiple-sinkers weight (CST vs. CSM).

Fig. 15 also indicates that the cage using multiple-sinker weight has a larger V_r than that using the sinker tube, but the differences of their V_r are less than 10% which agree with the previous work by Huang et al. (2007). Fig. 18 shows the deformation of these two types of fish cages under different current velocities. Similar to the observations from Fig. 17, the sinker tube can well maintain the shape of the bottom net but lead to a shallower net bag under strong current than that using multiple-sinker weight. Thus, CSM has a larger volume than CST when they have the same C , H , W and under the same U . However, the volume of sharp corners in CSM (circled in Fig. 12(b)), although included in the calculation, may not be used by fish due to their circular swimming pattern. In addition, the tension is usually large near the sharp corners, which may increase the risk of net failure. In contrast, as shown in Fig. 12(a), the sharp corners can be avoided in CST when the fish cage deforms. This can conform with the fish behaviours and may improve the fish welfare. Moreover, the sinker tube is able to better distribute the concentrated weight on the net and the floating collar. Thus, the risk of net failure can be reduced.

4.2.3. Effect of cage dimension on cultivation volume

Fish cages can be enlarged in the horizontal or vertical direction to accommodate more fish. However, the gained volume from the increment of the circumference or depth can significantly reduce with increasing current velocity. Although it is difficult to quantify the influence of circumference or depth on the cultivation volume in Fig. 19 due to a large number of cases, it can still observe that the cultivation

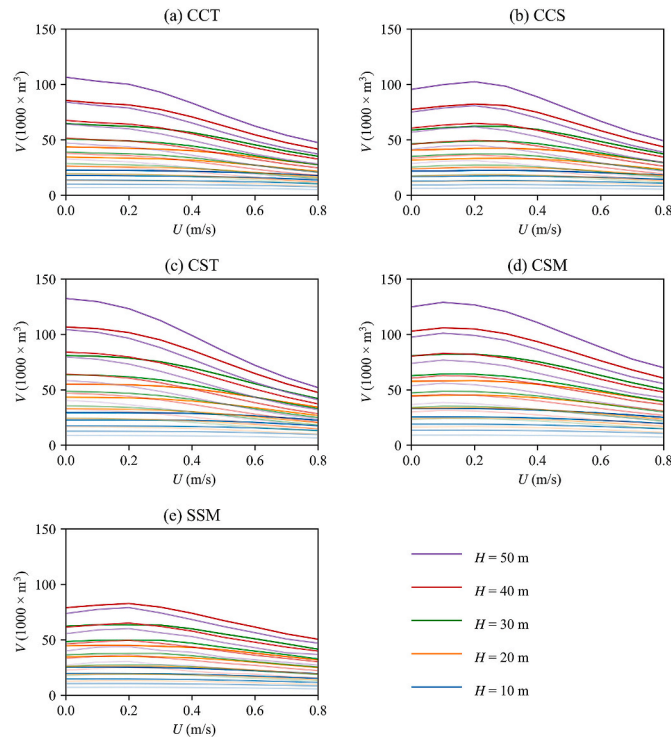


Fig. 19. Cultivation volumes of the five fish cages with $W = 60$ kg/m under different current velocities. The shades of colours (from light to dark) represent the different circumferences (C is from 100 m to 180 m). (For interpretation of the references to colour in this figure legend, the reader is referred to the Web version of this article.)

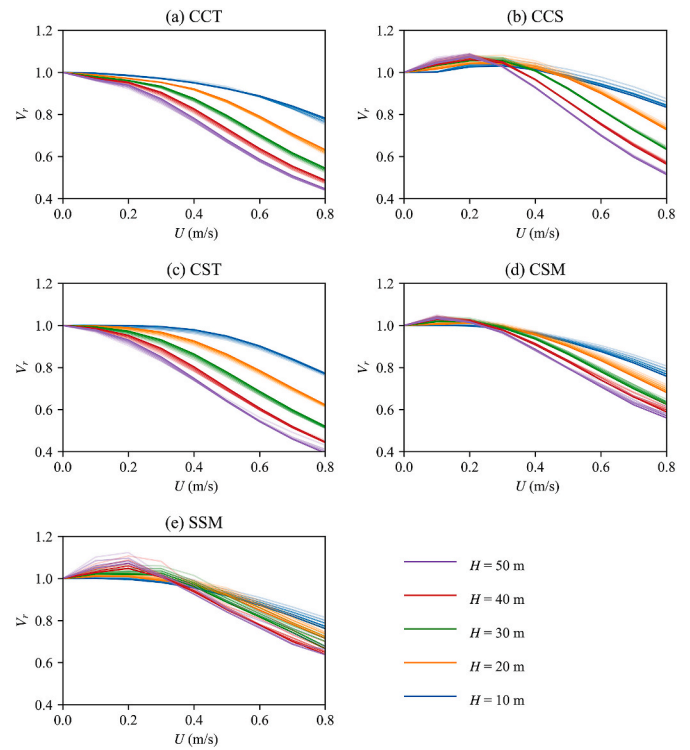


Fig. 20. Remaining volume factors for the five fish cages with $W = 60$ kg/m under different current velocities. The shades of colours (from light to dark) represent the circumferences (C is from 100 m to 180 m). (For interpretation of the references to colour in this figure legend, the reader is referred to the Web version of this article.)

volume of the large cages is reduced faster with the increasing current velocity than those of the small cages. For a better comparison, the effect of changing the circumference or depth on V_r is shown in Fig. 20.

For the CCT, CCS and CST cages, an increment of H can certainly increase V_0 but can significantly reduce V_r when the current is strong ($U > 0.4$ m/s). This means the volume gained from the increment of H can be lost under strong current, but the cost for construction is increased. However, an increment of C has little effect on V_r for CCT, CCS and CST cages, which means the volume gained from the increment of C can be well maintained even when the current is strong. Thus, it is suggested to enlarge the fish cage horizontally to gain more cultivation volume when the site has a strong current.

For the other two cages using multiple-sinker weight, i.e., CSM and SSM, the increment of H and C can both reduce V_r , and their effectiveness is roughly equivalent. Thus, the dimensions of these two fish cages may need to be determined based on the site conditions as well as the types of farmed fish.

4.2.4. Effect of net bag shape on cultivation volume

Although the cultivation volumes are reduced with different speeds under currents, the trend that the stouter cage has higher efficiency in material usage is still valid, as shown in Fig. 21. At the same time, increasing the fish cage dimension can also reduce the usage of netting per unit cultivation volume. In addition, it can be observed that CSM has a larger cultivation volume than CST when both net bags have the same dimension and use the same amount of weight. Thus, CSM has a higher efficiency in material usage than CST when the current is strong. The two types of cages using sinker tube, i.e., CCT and CST, have almost the same cultivation volume when both have the same H , C and W under the same U . As CCT use less netting, A_{net}/V of CCT is smaller than that of CST.

As shown in Fig. 22, an increment of H/C which will make the cage

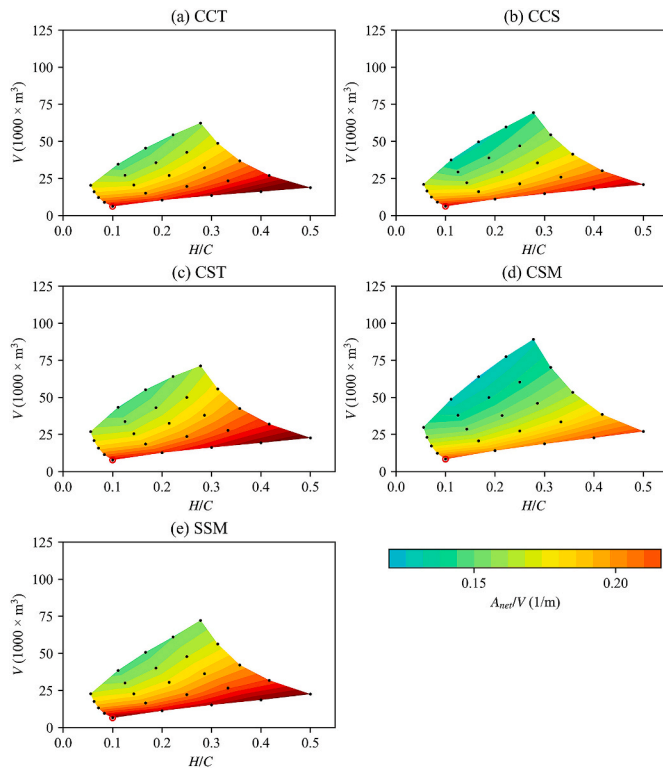


Fig. 21. Cultivation volumes of the five fish cage with $W = 40 \text{ kg/m}$ when $U = 0.5 \text{ m/s}$. The black points represent the studied cases. The red circles represent the case with $H = 10 \text{ m}$ and $C = 100 \text{ m}$. (For interpretation of the references to colour in this figure legend, the reader is referred to the Web version of this article.)

slimmer, can reduce V_r in general, meaning that the volume of the slim cage can be easily reduced by the current force. For all the cage types, larger cages have a smaller V_r than the smaller cages, meaning that the larger cages are usually easier to get volume reductions due to the current force. In addition, it can be observed that SSM has a relatively stable V_r , which does not change so much with H/C , compared to the other four cage types. It may be because the cultivation volume of this square cage is relatively small compared to the other cages with the same H , C and W under the same U .

4.3. Volume prediction under current conditions

In the preliminary design process, the cultivation volume is one of the most concerning aspects and usually needs to be updated several times based on the biomass and site conditions. Thus, a quick and accurate method to predict the cultivation volume is in need to reduce the workload. Based on the discussions in Sections 4.1 and 4.2, the cultivation volume of a fish cage under current conditions highly depends on its dimension, weight and the current-induced drag force, which can be characterised by the main design parameters H , C , W and U . According to Dong et al. (2021) and Moe-Føre et al. (2016), the dimensionless drag force F_d/W_0 and the remaining volume factor V_r have a strong negative correlation. Thus, the cultivation volume may be predicted if F_d/W_0 is known. However, the drag force F_d is not easy to be directly estimated based on the main design parameters. Usually, in order to get F_d , a series of scaled model experiments or verified numerical simulations need to be conducted, which will be costly and time-consuming. Thus, a superficial drag force F_d^* is proposed to replace F_d and employed in the regression function for the volume prediction. F_d^* is defined as Eq. (27) and has the same unit as F_d .

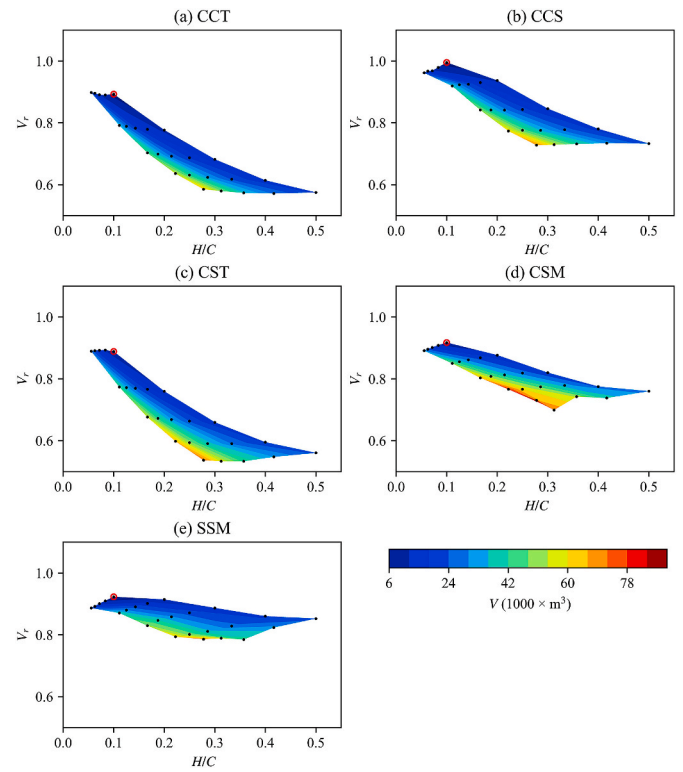


Fig. 22. Remaining volume factors for the fish cage with $W = 40 \text{ kg/m}$ when $U = 0.5 \text{ m/s}$. The black points represent the studied cases. The red circles represent the case with $H = 10 \text{ m}$ and $C = 100 \text{ m}$. (For interpretation of the references to colour in this figure legend, the reader is referred to the Web version of this article.)

Table 7

Regression coefficients for the volume prediction by Eq. (29).

Cage name	Coefficients		R^2
	a	b	
CCT	0.1710 ± 0.0019	0.9935 ± 0.0054	0.9933
CCS	0.1267 ± 0.0022	0.9047 ± 0.0064	0.9833
CST	0.1992 ± 0.0016	0.9738 ± 0.0047	0.9962
CSM	0.1035 ± 0.0027	0.9805 ± 0.0077	0.9645
SSM	0.0768 ± 0.0035	0.9802 ± 0.0099	0.9035

$$F_d^* = \frac{1}{2} \rho C_{D(\theta=0^\circ)} U^2 H C \quad (27)$$

where ρ is the density of the water, $C_{D(\theta=0^\circ)}$ is the drag coefficient of the netting when the current is perpendicular to the net panel (Eq. (7)), U is the current velocity, H is the designed depth of net bag and C is the designed circumference of floating collar.

The regression function for the cultivation volume is shown in Eq. (28). In the regression function, W_0 is the total submerged weight on a cage, which can be expressed as $W_0 = C \times g \times W$. Besides, V_r on the left side of Eq. (28) is inverted so that both sides of the equation will increase with the increasing current velocity. The regression analysis is conducted based on the data from the present simulation results and using the linear least squares method. The regression coefficients are listed in Table 7, and the regression results are shown in Fig. 23. Theoretically, the intercept b in regression functions should be 1, as $V = V_0$ when $U = 0 \text{ m/s}$ ($F_d^* = 0$). As shown in Fig. 23, although the five regression functions have different slopes, their intercepts are around 1.

$$\frac{1}{V_r} = a \frac{F_d^*}{W_0} + b \quad (28)$$

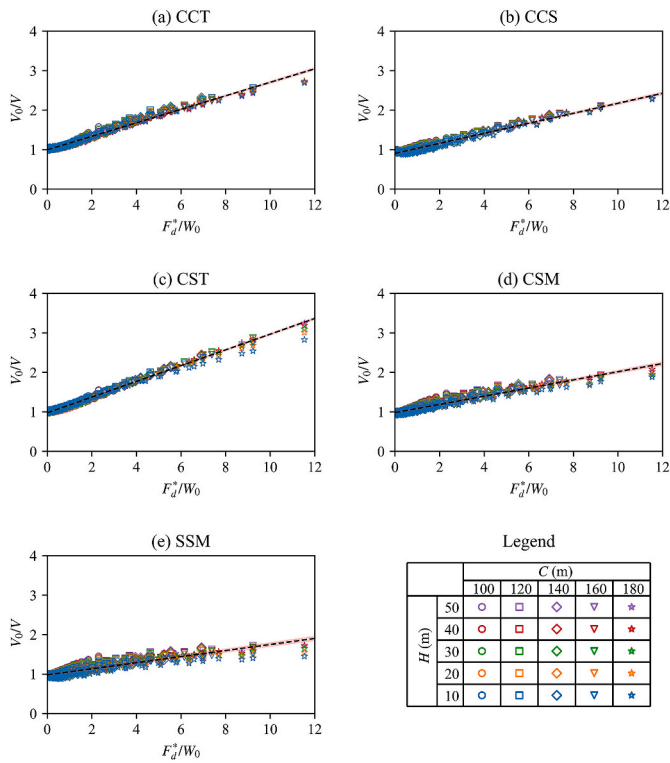


Fig. 23. Regression functions for volume predictions. The shadows show the 99.7% confidence intervals for the regression function in Eq. (29).

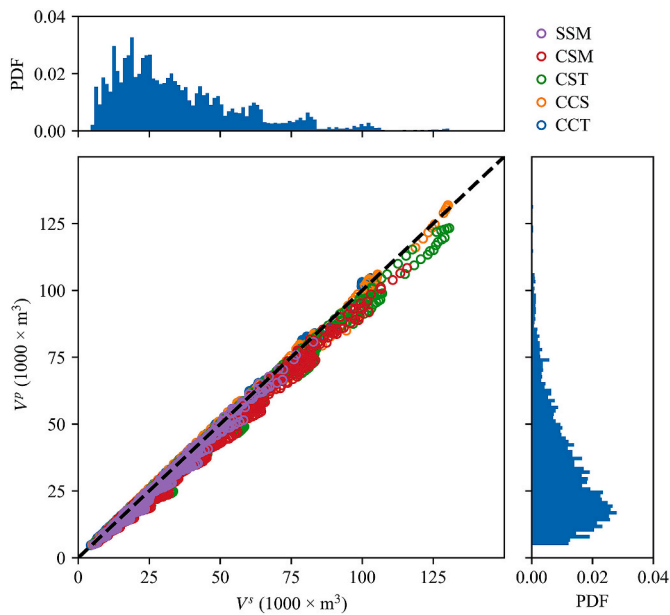


Fig. 24. The cultivation volumes predicted using Eq. (29) and the cultivation volume based on the present numerical simulations. The scatter plot on the left side includes the results from all the simulation cases: $5 \times 5 \times 5 \times 5 \times 9 = 5625$. The PDF means the probability density function. The right and top subplots show the probability density of the V^p and V^s for the data in the present study, respectively.

$$V = \frac{V_0 W_0}{a F_d^* + b W_0} \quad (29)$$

Based on the regression function in Eq. (28), the predicted cultivation volume can be expressed as a function of V_0 , W_0 and F_d^* in Eq. (29),

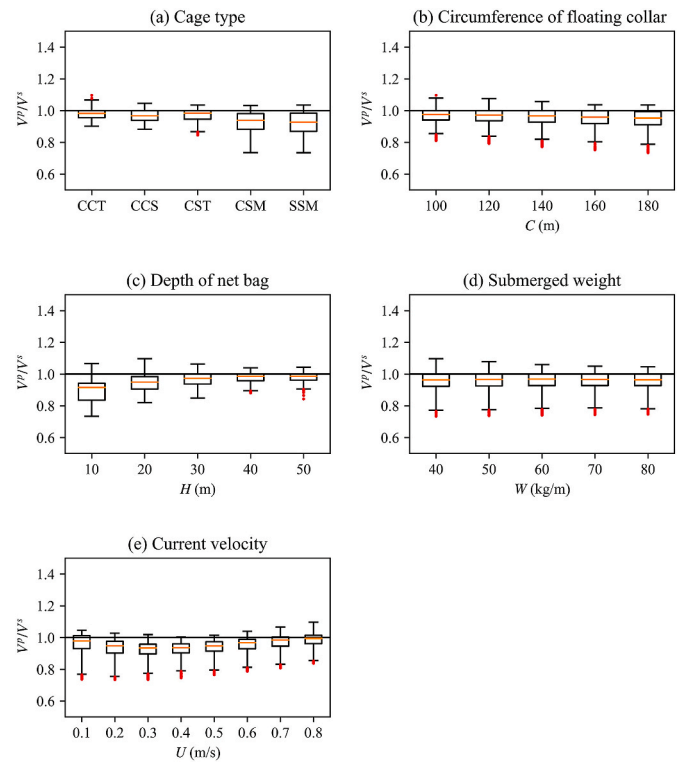


Fig. 25. Evaluation of the volume prediction function from different perspectives. The distributions of V^p/V^s are presented by boxplots.

where all the parameters are known in the preliminary design process. Using this formula, the cultivation volume for different fish cages under different current conditions can be easily predicted for various design purposes.

Fig. 24 compares the predicted cultivation volume (V^p) using Eq. (29) and the cultivation volume from numerical simulations (V^s). The PDF means the probability density function, showing the probability density of V^p and V^s for all the 5625 simulation cases. For all the five cage types, the difference between V^p and V^s are on average 5%, with a maximum difference of 9%. This indicates that the proposed volume prediction function has high accuracy and can be acceptable for a quick empirical estimation. As shown in Fig. 24, the probability distributions of V^p and V^s are similar, and most of the studied cases have cultivation volumes $< 80\,000\text{ m}^3$.

The accuracy of predictions using Eq. (29) may be different with respect to cage types and the key design parameters. In order to evaluate the accuracy of Eq. (29), the distributions of V^p/V^s are presented in Fig. 25 from the perspectives of cage type, C , H , W and U . In terms of cage type, V^p/V^s of the cages using multiple-sinker weight, *i.e.*, CSM and SSM, have a relatively larger range compared to the other three cage types. This may be because the deformed CSM and SSM have sharp corners, as shown in Fig. 12, that may bring uncertainties to the volume predictions. In terms of cage dimensions, the accuracy of volume predictions is almost independent of C but can be influenced by H . The accuracy of volume predictions for the deep cages is higher than those for the short cages. In terms of W , the accuracy of volume predictions has almost the same variation for different W . In terms of U , the accuracy of the volume prediction first decreases with the increasing current velocity when $U < 0.3\text{ m/s}$, then increases with the increasing current velocity. This nonlinear relationship may be caused by the quadratic velocity term in the hydrodynamic model and wake effects.

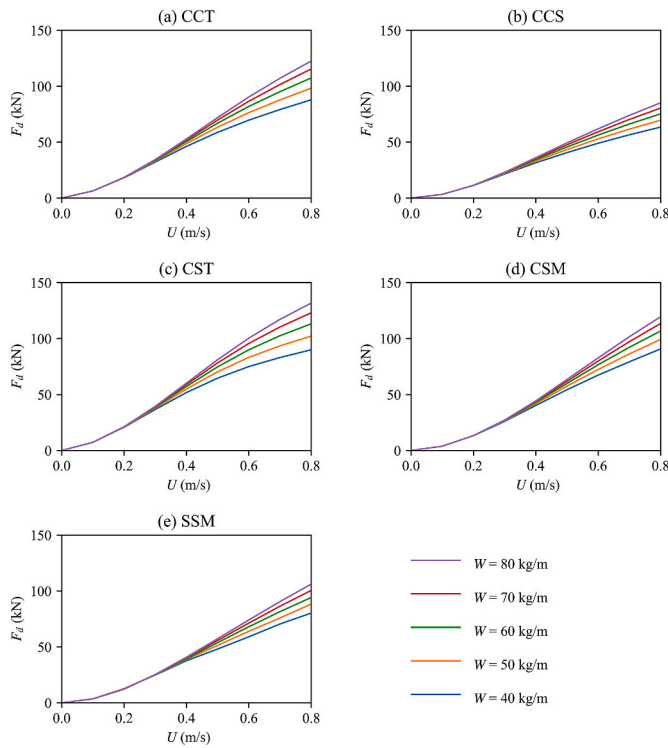


Fig. 26. Drag forces on the fish cages with $C = 140$ m and $H = 30$ m under different current velocities.

4.4. Drag force under current conditions

4.4.1. Effect of current velocity on drag force

Fig. 26 shows the drag force on the net bag of the five types of fish cages under different current velocities. Their drag forces increase with the increasing current velocity, and the increasing speeds of drag forces decrease with the increasing current velocity. This is caused by the deformations of the flexible cage net as well as the wake effects. Although the velocity is a quadratic term in the hydrodynamic models, the deformed cages cause a reduced projected area of the fish cage net. Together with the wake effects, which cause a reduced velocity on the downstream nets, the drag force increases slower with the increasing current velocity.

4.4.2. Effect of weight system on drag force

Fig. 26 also shows that increasing the W will increase the F_d on the fish cage, especially when $U > 0.5$ m/s. For the small to moderate current velocity $U < 0.5$ m/s, F_d on a fish cage with W are almost equal because the cages have similar deformed shapes under that small current force. For high current velocity $U > 0.5$ m/s, the increment of W has an obvious effect on the volume maintenance, as discussed in Section 4.2.2. However, the additional cultivation volume caused by increasing W is gained in exchange for additional F_d on the fish cages. Thus, the requirement for the mooring system needs to be increased to withstand a larger F_d if the W is increased.

The forms of weight can affect the F_d on a fish cage. Taking CCT and CCS as examples, F_d on the cage using sinker tube is much larger than that using single-sinker weight when both cages have the same dimension, amount of weight and under the same current velocity. The reason why the sinker tube causes a larger F_d than the single-sinker weight may be that the net bag's shape of the one using sinker tube is well kept, and this results in a larger project area than that using single-sinker weight. Subsequently, based on the comparisons between CST and CSM, the sinker tube does not cause a larger F_d than the multiple-sinker weight.

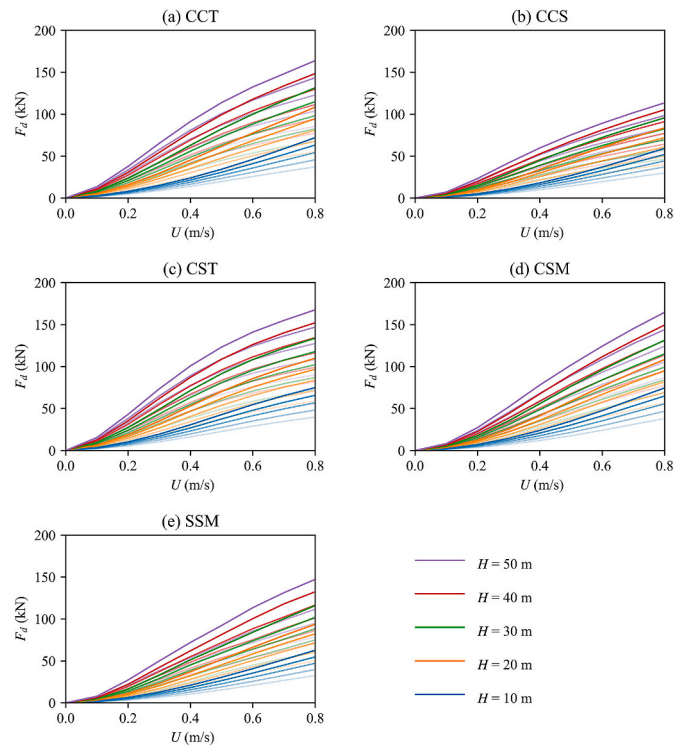


Fig. 27. Drag forces on the fish cages with $W = 50$ kg/m under different current velocities. The shades of colours (from light to dark) represent the different circumferences (C is from 100 m to 180 m). (For interpretation of the references to colour in this figure legend, the reader is referred to the Web version of this article.)

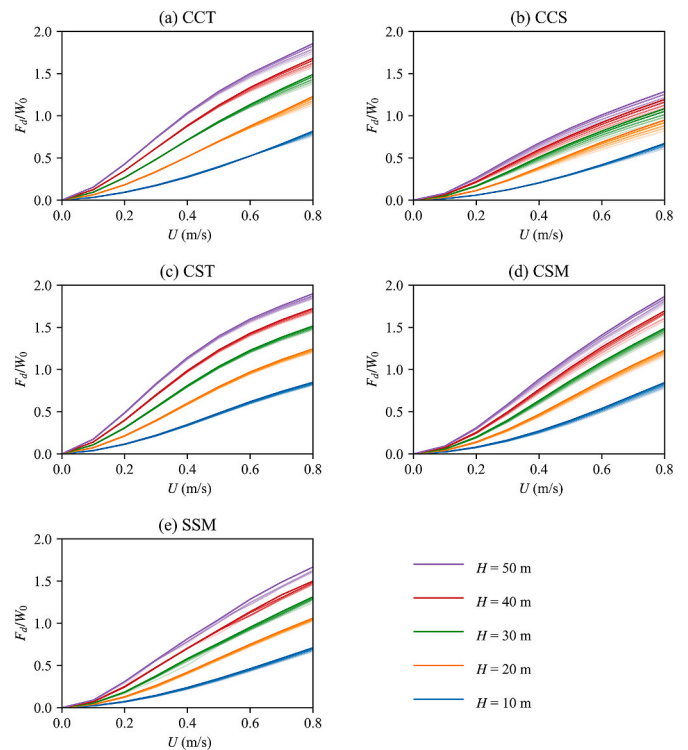


Fig. 28. F_d/W_0 of the fish cages with $W = 50$ kg/m under different current velocities. The shades of colours (from light to dark) represent the different circumferences (from 100 m to 180 m). (For interpretation of the references to colour in this figure legend, the reader is referred to the Web version of this article.)

4.4.3. Effect of cage dimension on drag force

As shown in Fig. 27, when the dimension of a fish cage is increased, no matter horizontally or vertically, F_d on the net bag will increase significantly, especially when U is large. Due to the large number of simulation cases, curves of F_d overlap each other in Fig. 27, and it is difficult to quantify the effects of C or H on F_d . Thus, the dimensionless F_d/W_0 is used for better comparison, as shown in Fig. 28.

As shown in Fig. 28, except for CCS, the increment of C has negligible effects on F_d/W_0 for the other four types of fish cage. This means the increment of F_d caused by increasing C are roughly equal to the increment of W_0 . As W_0 has a linear relationship with C ($W_0 = C \times g \times W$), the F_d on the net bag should also have almost a linear relationship with C . Because F_d/W_0 is almost independent of C , the value of for the four types of cage may be also independent of C , which are in accordance with the results in Fig. 20 as well as the observations by Mjåtveit et al. (2021). However, the increment of H can certainly increase F_d as well as F_d/W_0 , as W_0 does not depend on H . The increments of F_d (or F_d/W_0) are reduced with the increasing H . This nonlinear relationship between F_d (or F_d/W_0) and H may be caused by the deformation of net bags. When H is large, it is easy to have large deformation of the net bag under the current forces. Thus, the cage becomes much shallower than its designed H , and F_d on this shallow net bag is reduced significantly. Consequently, the increments of F_d become smaller with the increasing H . For CCS, increasing C or H can both increase F_d/W_0 in a similar way when $H > 10$ m. This phenomenon may be caused by the truncated-cone shape net bag and the single-sinker weight. As the single-sinker weight is located at a deep position, the fish cage shapes can be well kept, which are in accordance with the results in Fig. 20. Thus, F_d will increase faster than W_0 with the increasing C .

4.4.4. Effect of net bag shape on drag force

As shown in Fig. 29(b), F_d on CCS does not have a strong correlation with H/C , which means no matter the CCS cage is slim or stout, its F_d is

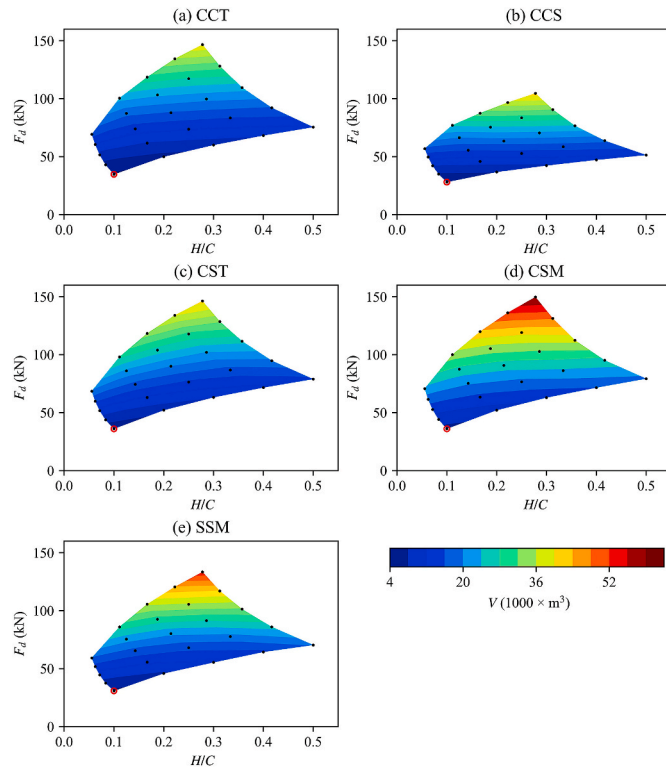


Fig. 29. Drag forces on the fish cages with $W = 40$ kg/m when $U = 0.8$ m/s. The black points represent the studied cases. The red circles represent the case with $H = 10$ m and $C = 100$ m. (For interpretation of the references to colour in this figure legend, the reader is referred to the Web version of this article.)

Table 8

Regression coefficients for the drag force prediction by Eq. (31).

Cage name	Coefficients		RMSE ^a
	a	b	
CCT	0.5522 ± 0.0081	0.5730 ± 0.0099	0.0686
CCS	0.3781 ± 0.0068	0.5715 ± 0.0120	0.0570
CST	0.6186 ± 0.0093	0.5410 ± 0.0102	0.0787
CSM	0.4837 ± 0.0072	0.6310 ± 0.0098	0.0611
SSM	0.4380 ± 0.0060	0.6287 ± 0.0090	0.0498

^a RMSE: Root mean square error.

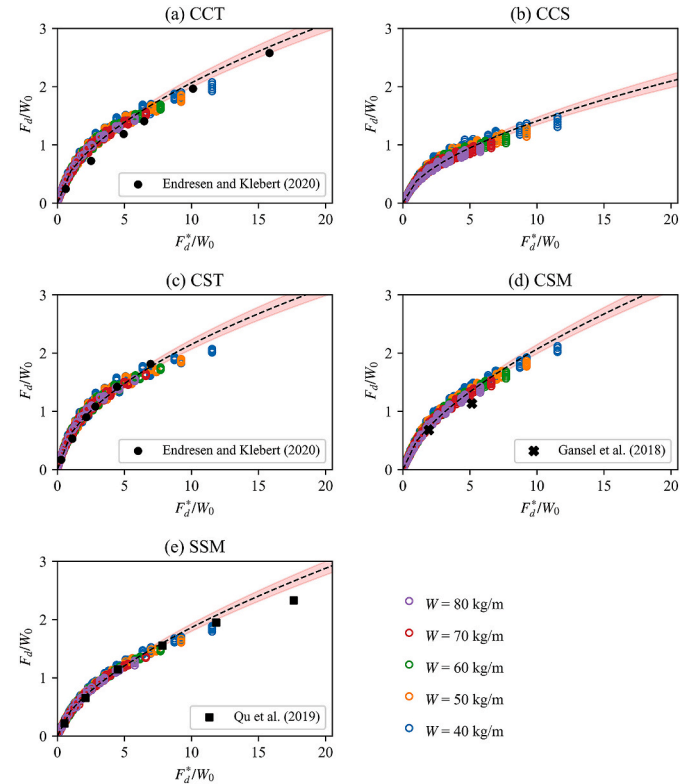


Fig. 30. Regression functions for drag force predictions. The shadows show the 99.7% confidence intervals for the regression function in Eq. (31).

only proportional to its cultivation volume. The other four types of fish cages also have this similar colour shades when their $V > 40\,000$ m³. However, when $V < 40\,000$ m³, F_d on the net bag is smaller if the cage is stouter (i.e., smaller H/C) with the same cultivation volume. The cage using sinker tube has a relatively smaller V/F_d , compared to the other three types of cage. This indicates that using sinker tube can significantly increase F_d on a fish cage. In addition, it can be observed that CSM has the largest cultivation volume as well as the largest drag force when the five cages have the same C , H , W and under the same U .

4.5. Drag force prediction under current conditions

Based on the discussions in Section 4.4, the drag force on a fish cage highly depends on H , C , W and U . In order to quickly predict the drag force on fish cages in the preliminary design process, a formula is proposed in this section based on regression analysis.

The regression function is shown in Eq. (30). The regression analysis is conducted based on the drag forces from the present simulation results and using the nonlinear least squares method. The regression coefficients are listed in Table 8, and the regression results are shown in Fig. 30. In addition to the present numerical results, external data from experiments (Endresen and Klebert, 2020; Qu et al., 2019) and sea trials

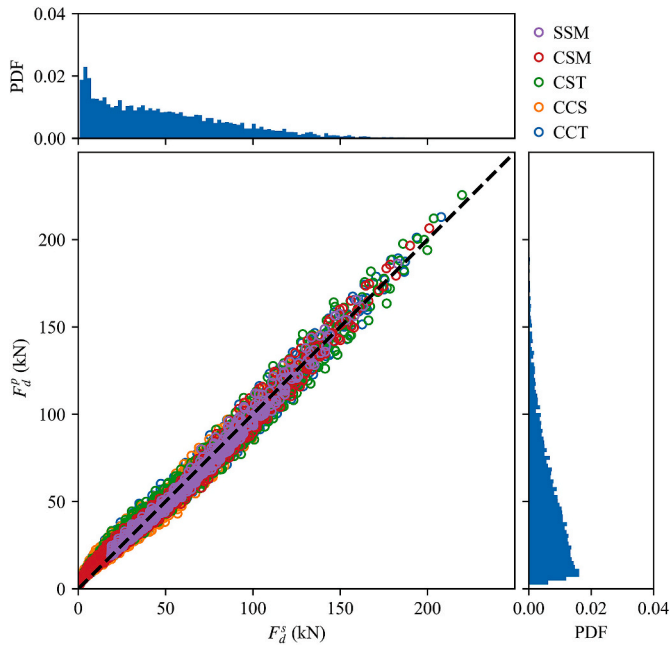


Fig. 31. The drag forces predicted using Eq. (31) and the drag forces based on the present numerical simulations. The scatter plot on the left side includes the results from all the simulation cases: $5 \times 5 \times 5 \times 5 \times 9 = 5\,625$. The PDF means the probability density function. The right and top subplots show the probability density of the F_d^p and F_d^s for the data in the present study, respectively.

(Gansel et al., 2018) are also included in Fig. 30 for reference.

$$\frac{F_d}{W_0} = a \left(\frac{F_d^*}{W_0} \right)^b \quad (30)$$

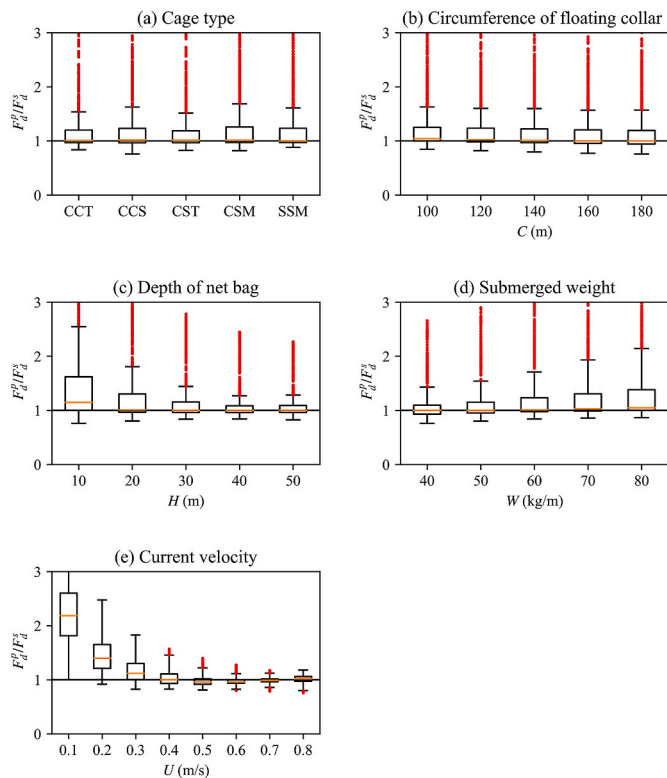


Fig. 32. Evaluation of the drag force prediction function from different perspectives. The distributions of F_d^p/F_d^s are presented by boxplots.

$$F_d = aW_0 \left(\frac{F_d^*}{W_0} \right)^b \quad (31)$$

Based on the regression function in Eq. (30), the predicted drag force can be expressed by Eq. (31), where all the parameters on the right side of this equation are known in the preliminary design process. Fig. 31 shows the comparison between the predicted drag force (F_d^p) using Eq. (31) and the drag force from numerical simulations (F_d^s). The PDF means the probability density function, showing the probability density of F_d^p and F_d^s for all the 5 625 simulation cases. On average, F_d^p is 24% higher than F_d^s . However, the difference between F_d^p and F_d^s is less than 2% on average when $F_d > 50$ kN. According to the probability distributions of F_d^s , the drag force on the net bag is less than 50 kN for 58% of the studied cases. Due to this considerable proportion of the cases with small drag forces, the overall difference between F_d^p and F_d^s is relatively large. Thus, when a fish cage has a small dimension or is under a small current, using Eq. (31) for the drag force prediction can make the structural design conservative. When the fish cage is large and under strong current, Eq. (31) can provide high-accuracy predictions on the drag force without any time-consuming simulation.

In order to evaluate the accuracy of the drag force predictions using Eq. (31), the distributions of F_d^p/F_d^s are presented in Fig. 32 from the perspectives of cage type, C , H , W and U . The most noticeable finding is from Fig. 32(e), in which F_d^p/F_d^s rapidly approaches 1 with the increasing U . This finding agrees well with the earlier observations in Fig. 31, which shows that the drag force can be overpredicted when $U < 0.3$ m/s, but can be accurately predicted when $U > 0.3$ m/s. Due to these overpredicted drag forces when $U < 0.3$ m/s, there are many data points located above the upper whiskers of the boxplots in Fig. 32(a)–(d). Although there are so many outliers in Fig. 32(a)–(d), the boxplots indicate that most of the predicted drag forces using Eq. (31) are very close to the drag forces obtained from numerical simulations. Based on Fig. 32 (a)–(b), the accuracy of drag force predictions is almost independent of cage types and C . Based on Fig. 32(c), the accuracy of the drag force predictions for the deep fish cages has a smaller variation and is higher than those of shallow fish cages. Based on Fig. 32(d), the accuracy of the drag force predictions for the cage with different W is similar on average, but the accuracy for the cage with larger W has a larger variation.

5. Conclusions

The main objective of the present study is to investigate the structural responses of commonly used gravity fish cages and provide guides for future structural design. This study provides a comprehensive assessment on the effects of the design parameters, including circumference of the floating collar, depth of net bag, forms of weight and current velocity, on the cultivation volumes and drag forces. The following conclusions are drawn from the results:

1. A stout fish cage, no matter square or circular shape, can efficiently use the materials and provide a larger cultivation volume than a slim fish cage when the two cages use the same amount of netting, weight and are under the same strong current ($U > 0.4$ m/s) condition. Thus, increasing circumference is more effective than increasing the depth of net bag to improve cultivation volume.
2. Given the same circumference of floating collar, depth of net bag, amount of weight and current velocity, the square fish cage has a smaller cultivation volume than the circular one, although it has a slightly larger remaining volume factor.
3. An increment of submerged weight can mitigate the cage deformation and help to maintain cultivation volume under strong current, but bring negligible improvements of cultivation volume when current velocity is lower than 0.2 m/s.

4. Sinkers can maintain the net bag shape well under current conditions. However, due to the upward movement of the bottom net, the cultivation volume can significantly decrease under strong current conditions.
5. Multiple-sinker weight shows the best performance in the volume maintenance, especially when the current velocity is large. However, multiple-sinker weight can cause irregular bottom and front nets, in which the space may be hardly used by the farmed fish and the risk of net failure may be increased.
6. With a constant submerged weight per meter, the drag force on fish cages almost linearly increases with the increasing circumference, but nonlinearly increases with the increasing current velocity and depth of net bag.
7. The drag forces on the cages using sinker tube and multiple-sinker weight are roughly equal, when the five types of fish cage have the same circumference of floating collar, depth of net bag, amount of weight and are under the same current velocity condition. Meanwhile, the drag forces on cages using single-sinker weight are much smaller than those using other forms of weight under the same condition.

In addition to the above findings, multiple regression analyses are conducted based on a large number of numerical results. The regression functions can provide high-accuracy predictions for the most concerning aspects in the preliminary design process, and it can save considerable time for experiments and numerical simulations in the cage design.

Besides, a hydrodynamic library, namely UiS-Aqua, is developed for the dynamic analysis of aquaculture structures, and this library is open access at GitHub. The open-source library can serve as a base for future studies and save considerable time for the code development in dynamic analysis of fish cages. Moreover, the library developed in the present study can also be applied to fishing gears and marine structures, such as trawl net, seine net, raft culture and subsea cable.

CRedit authorship contribution statement

Hui Cheng: Conceptualization, Methodology, Software, Validation, Formal analysis, Investigation, Data curation, Writing – original draft, Writing – review & editing, Visualization. **Lin Li:** Conceptualization, Investigation, Formal analysis, Writing – review & editing, Supervision. **Muk Chen Ong:** Conceptualization, Investigation, Formal analysis, Resources, Writing – review & editing, Supervision, Project administration, Funding acquisition.

Declaration of competing interest

The authors declare that they have no known competing financial interests or personal relationships that could have appeared to influence the work reported in this paper.

Acknowledgements

The authors would like to thank Digvijay Patankar from the Indian Institute of Technology, Jean Pierre Aubry from La Machine and the anonymous in the Code_Aster forum for providing help in using Code_Aster.

References

- AKVA Group, 2020. *Pen Farming Aquaculture Catalogue (English)*.
 Berstad, A.J., Tronstad, H., Sivertsen, S.-A., Leite, E., 2008. Enhancement of design criteria for fish farm facilities including operations. In: Presented at the ASME 2005 24th International Conference on Offshore Mechanics and Arctic Engineering. American Society of Mechanical Engineers Digital Collection, pp. 825–832. <https://doi.org/10.1115/OMAE2005-67451>.
 Berstad, A.J., Walaunet, J., Heimstad, L.F., 2013. Loads from currents and waves on net structures. In: Presented at the ASME 2012 31st International Conference on Ocean, Offshore and Arctic Engineering. American Society of Mechanical Engineers Digital Collection, pp. 95–104. <https://doi.org/10.1115/OMAE2012-83757>.
 Berstad, A.J., Heimstad, L.F., Walaunet, J., 2014. Model testing of fish farms for validation of analysis programs. In: Presented at the ASME 2014 33rd International Conference on Ocean, Offshore and Arctic Engineering. American Society of Mechanical Engineers Digital Collection. <https://doi.org/10.1115/OMAE2014-24647>.
 Beveridge, M.C.M., 2004. *Cage Aquaculture*, third ed. Oxford, UK. Blackwell Pub, Ames, Iowa.
 Bi, C.-W., Xu, T.-J., 2018. Numerical study on the flow field around a fish farm in tidal current. *Turk. J. Fish. Aquat. Sci.* 18 https://doi.org/10.4194/1303-2712-v18_5_06.
 Bi, C.-W., Zhao, Y.-P., Dong, G.-H., Cui, Y., Gui, F.-K., 2015. Experimental and numerical investigation on the damping effect of net cages in waves. *J. Fluid Struct.* 55, 122–138. <https://doi.org/10.1016/j.jfluidstructs.2015.02.010>.
 Bi, C.-W., Zhao, Y.-P., Dong, G.-H., 2020. Experimental study on the effects of farmed fish on the hydrodynamic characteristics of the net cage. *Aquaculture* 524, 735239. <https://doi.org/10.1016/j.aquaculture.2020.735239>.
 Buck, B.H., Langan, R. (Eds.), 2017. *Aquaculture Perspective of Multi-Use Sites in the Open Ocean*. Springer International Publishing, Cham. <https://doi.org/10.1007/978-3-319-51159-7>.
 Cardia, F., Lovatelli, A., 2015. *Aquaculture Operations in Floating HDPE Cages: a Field Handbook*. Food and Agriculture Organization of the United States, Rome.
 Cha, B.-J., Lee, C.-W., 2002. Dynamic simulation of a midwater trawl system's behavior. *Fish. Sci.* 68, 1865–1868. https://doi.org/10.2331/fishsci.68.sup2_1865.
 Cha, B.-J., Lee, G.-H., 2018. Performance of a model fish cage with copper-alloy net in a circulating water channel and wave tank. *Ocean. Eng.* 151, 290–297. <https://doi.org/10.1016/j.oceaneng.2018.01.053>.
 Chen, D., Wang, C.M., Zhang, H., 2021. Examination of net volume reduction of gravity-type open-net fish cages under sea currents. *Aquacult. Eng.* 92, 102128. <https://doi.org/10.1016/j.aquaeng.2020.102128>.
 Cheng, H., Huang, L., Ni, Y., Xu, Q., Zhao, F., Wang, X., Liang, Z., 2018. Numerical and experimental study of SPM fish cage: comparison and validation. In: Presented at the ASME 2018 37th International Conference on Ocean, Offshore and Arctic Engineering. American Society of Mechanical Engineers Digital Collection. <https://doi.org/10.1115/OMAE2018-78204>.
 Cheng, H., Aarsæther, K.G., Li, L., Ong, M.C., 2020a. Numerical study of a single-point mooring gravity fish cage with different deformation-suppression methods. *J. Offshore Mech. Arctic Eng.* 142, 041301 <https://doi.org/10.1115/1.4046115>.
 Cheng, H., Li, L., Aarsæther, K.G., Ong, M.C., 2020b. Typical hydrodynamic models for aquaculture nets: a comparative study under pure current conditions. *Aquacult. Eng.* 90, 102070. <https://doi.org/10.1016/j.aquaeng.2020.102070>.
 Cheng, H., Li, L., Ong, M.C., Aarsæther, K.G., Sim, J., 2021. Effects of mooring line breakage on dynamic responses of grid moored fish farms under pure current conditions. *Ocean. Eng.* 237, 109638. <https://doi.org/10.1016/j.oceaneng.2021.109638>.
 Chu, Y.L., Wang, C.M., Park, J.C., Lader, P.F., 2020. Review of cage and containment tank designs for offshore fish farming. *Aquaculture* 519, 734928. <https://doi.org/10.1016/j.aquaculture.2020.734928>.
 Costello, C., Cao, L., Gelcich, S., Cisneros-Mata, M.Á., Free, C.M., Froehlich, H.E., Golden, C.D., Ishimura, G., Maier, J., Macadam-Somer, I., Mangin, T., Melnychuk, M.C., Miyahara, M., de Moor, C.L., Naylor, R., Nøstbakken, L., Ojeda, E., O'Reilly, E., Parma, A.M., Plantinga, A.J., Thilsted, S.H., Lubchenco, J., 2020. The future of food from the sea. *Nature* 588, 95–100. <https://doi.org/10.1038/s41586-020-2616-y>.
 Davis, K.F., Gephart, J.A., Emery, K.A., Leach, A.M., Galloway, J.N., D'Odorico, P., 2016. Meeting future food demand with current agricultural resources. *Global Environ. Change* 39, 125–132. <https://doi.org/10.1016/j.gloenvcha.2016.05.004>.
 DeCew, J., Tsukrov, I., Risso, A., Swift, M.R., Celikkol, B., 2010. Modeling of dynamic behavior of a single-point moored submersible fish cage under currents. *Aquacult. Eng.* 43, 38–45. <https://doi.org/10.1016/j.aquaeng.2010.05.002>.
 Dong, S., You, X., Hu, F., 2021. Experimental investigation on the fluid–structure interaction of a flexible net cage used to farm Pacific bluefin tuna (*Thunnus orientalis*). *Ocean. Eng.* 226, 108872. <https://doi.org/10.1016/j.oceaneng.2021.108872>.
 Edwards, P., 2015. Aquaculture environment interactions: past, present and likely future trends. *Aquaculture* 447, 2–14. <https://doi.org/10.1016/j.aquaculture.2015.02.001>.
 Endresen, P.C., Klebert, P., 2020. Loads and response on flexible conical and cylindrical fish cages: a numerical and experimental study based on full-scale values. *Ocean. Eng.* 216, 107672. <https://doi.org/10.1016/j.oceaneng.2020.107672>.
 Endresen, P.C., Birkevold, J., Føre, M., Fredheim, A., Kristiansen, D., Lader, P., 2014. Simulation and validation of a numerical model of a full aquaculture net-cage system. In: *Ocean Space Utilization; Professor Emeritus J. Randolph Paulling Honoring Symposium on Ocean Technology*. Presented at the ASME 2014 33rd International Conference on Ocean, Offshore and Arctic Engineering, vol. 7. American Society of Mechanical Engineers, San Francisco, California, USA. <https://doi.org/10.1115/OMAE2014-23382.V007T05A006>.
 FAO, 2020a. In: *Fishery and Aquaculture Statistics 2018*, FAO Yearbook of Fishery and Aquaculture Statistics. FAO, Rome, Italy. <https://doi.org/10.4060/cb1213t>.
 FAO, 2020b. In: *The State of World Fisheries and Aquaculture 2020: Sustainability in Action, the State of World Fisheries and Aquaculture (SOFIA)*. FAO, Rome, Italy. <https://doi.org/10.4060/ca9229en>.
 FAO, IFAD, UNICEF, WFP, WHO, 2020. *The state of food security and nutrition in the world 2020, transforming food systems for affordable healthy diets*. FAO, IFAD, UNICEF, WFP and WHO. <https://doi.org/10.4060/ca9692en>.

- Froehlich, H.E., Gentry, R.R., Halpern, B.S., 2018. Global change in marine aquaculture production potential under climate change. *Nat Ecol Evol* 2, 1745–1750. <https://doi.org/10.1038/s41559-018-0669-1>.
- Gansel, L.C., Oppedal, F., Birkeveld, J., Tuene, S.A., 2018. Drag forces and deformation of aquaculture cages—full-scale towing tests in the field. *Aquacult. Eng.* 81, 46–56. <https://doi.org/10.1016/j.aquaeng.2018.02.001>.
- Guo, Y.C., Mohapatra, S.C., Guedes Soares, C., 2020. Review of developments in porous membranes and net-type structures for breakwaters and fish cages. *Ocean. Eng.* 200, 107027. <https://doi.org/10.1016/j.oceaneng.2020.107027>.
- Halwart, M., Soto, D., Arthur, J.R. (Eds.), 2007. *Cage Aquaculture: Regional Reviews and Global Overview*. FAO, Rome. FAO fisheries technical paper.
- Huang, C.-C., Tang, H.-J., Liu, J.-Y., 2007. Modeling volume deformation in gravity-type cages with distributed bottom weights or a rigid tube-sinker. *Aquacult. Eng.* 37, 144–157. <https://doi.org/10.1016/j.aquaeng.2007.04.003>.
- Huang, X.-H., Liu, H.-Y., Hu, Y., Yuan, T.-P., Tao, Q.-Y., Wang, S.-M., Liu, Z.-X., 2020. Hydrodynamic performance of a semi-submersible offshore fish farm with a single point mooring system in pure waves and current. *Aquacult. Eng.* 90, 102075. <https://doi.org/10.1016/j.aquaeng.2020.102075>.
- Huguenin, J.E., 1997. The design, operations and economics of cage culture systems. *Aquacult. Eng.* 16, 167–203. [https://doi.org/10.1016/S0144-8609\(96\)01018-7](https://doi.org/10.1016/S0144-8609(96)01018-7).
- Johannesen, Å., Patursson, Ø., Kristmundsson, J., Dam, S.P., Mulelid, M., Klebert, P., 2021. Waves and currents decrease the available space in a salmon cage (preprint). *Anim. Behav. Cogn.* <https://doi.org/10.1101/2021.07.23.453560>.
- Klebert, P., Lader, P., Gansel, L., Oppedal, F., 2013. Hydrodynamic interactions on net panel and aquaculture fish cages: a review. *Ocean. Eng.* 58, 260–274. <https://doi.org/10.1016/j.oceaneng.2012.11.006>.
- Knysh, A., Tsukrov, I., Chambers, M., Swift, M.R., Sullivan, C., Drach, A., 2020. Numerical modeling of submerged mussel longlines with protective sleeves. *Aquacult. Eng.* 88, 102027. <https://doi.org/10.1016/j.aquaeng.2019.102027>.
- Knysh, A., Coyle, J., DeCew, J., Drach, A., Swift, M.R., Tsukrov, I., 2021. Floating protective barriers: evaluation of seaworthiness through physical testing, numerical simulations and field deployment. *Ocean. Eng.* 227, 108707. <https://doi.org/10.1016/j.oceaneng.2021.108707>.
- Kristiansen, T., 2013. A numerical parameter study on current forces on circular aquaculture net cages. In: Presented at the ASME 2013 32nd International Conference on Ocean, Offshore and Arctic Engineering. American Society of Mechanical Engineers Digital Collection. <https://doi.org/10.1115/OMAE2013-10915>.
- Kristiansen, T., Faltinsen, O.M., 2012. Modelling of current loads on aquaculture net cages. *J. Fluid Struct.* 34, 218–235. <https://doi.org/10.1016/j.jfluidstruct.2012.04.001>.
- Lader, P.F., Enerhaug, B., 2005. Experimental investigation of forces and geometry of a net cage in uniform flow. *IEEE J. Ocean. Eng.* 30, 79–84. <https://doi.org/10.1109/JOE.2004.841390>.
- Lader, P., Jensen, A., Sveen, J.K., Fredheim, A., Enerhaug, B., Fredriksson, D., 2007a. Experimental investigation of wave forces on net structures. *Appl. Ocean Res.* 29, 112–127. <https://doi.org/10.1016/j.apor.2007.10.003>.
- Lader, P., Olsen, A., Jensen, A., Sveen, J.K., Fredheim, A., Enerhaug, B., 2007b. Experimental investigation of the interaction between waves and net structures—damping mechanism. *Aquacult. Eng.* 37, 100–114. <https://doi.org/10.1016/j.aquaeng.2007.03.001>.
- Lee, C.-W., 2002. Dynamic analysis and control technology in a fishing gear system. *Fish. Sci.* 68, 1835–1840. <https://doi.org/10.2331/fishsci.68.sup2.1835>.
- Lee, C.-W., Kim, Y.-B., Lee, G.-H., Choe, M.-Y., Lee, M.-K., Koo, K.-Y., 2008. Dynamic simulation of a fish cage system subjected to currents and waves. *Ocean. Eng.* 35, 1521–1532. <https://doi.org/10.1016/j.oceaneng.2008.06.009>.
- Lee, C.W., Lee, G.H., Choe, M.Y., Song, D.H., Hosseini, S.A., 2010. In: Dynamic Behavior of a Submersible Fish Cage. Presented at the ASME 2009 28th International Conference on Ocean, Offshore and Arctic Engineering. American Society of Mechanical Engineers Digital Collection, pp. 201–206. <https://doi.org/10.1115/OMAE2009-79328>.
- Lee, C.W., Lee, J., Park, S., 2015. Dynamic behavior and deformation analysis of the fish cage system using mass-spring model. *China Ocean Eng.* 29, 311–324. <https://doi.org/10.1007/s13344-015-0022-2>.
- Lekang, O.-I., 2019. *Aquaculture Engineering*, third ed. Wiley-Blackwell, Hoboken.
- Li, Y.-C., Zhao, Y.-P., Gui, F.-K., Teng, B., Dong, G.-H., 2006a. Numerical simulation of the influences of sinker weight on the deformation and load of net of gravity sea cage in uniform flow. *hyxb* 125–137.
- Li, Y.-C., Zhao, Y.-P., Gui, F.-K., Teng, B., Guan, C.-T., 2006b. Numerical analysis of the effects of sinker weight on the hydrodynamics behaviour of gravity cage net in uniform flow. *J. Hydrodyn. Ser. B, Proc. Confer. Global Chin. Scholars Hydrodyn.* 18, 77–83. [https://doi.org/10.1016/S1001-6058\(06\)60034-6](https://doi.org/10.1016/S1001-6058(06)60034-6).
- Mjåtteit, M.A., Cheng, H., Ong, M.C., Lee, J., 2021. Numerical study of two typical gravity-based fish cages with different dimensions under pure current conditions. *Aquacult. Eng.* (under view).
- Moe-Føre, H., Lader, P.F., Lien, E., Hopperstad, O.S., 2016. Structural response of high solidity net cage models in uniform flow. *J. Fluid Struct.* 65, 180–195. <https://doi.org/10.1016/j.jfluidstruct.2016.05.013>.
- Naylor, R.L., Goldberg, R.J., Primavera, J.H., Kautsky, N., Beveridge, M.C.M., Clay, J., Folke, C., Lubchenco, J., Mooney, H., Troell, M., 2000. Effect of aquaculture on world fish supplies. *Nature* 405, 1017–1024. <https://doi.org/10.1038/35016500>.
- Naylor, R.L., Hardy, R.W., Buschmann, A.H., Bush, S.R., Cao, L., Klinger, D.H., Little, D. C., Lubchenco, J., Shumway, S.E., Troell, M., 2021. A 20-year retrospective review of global aquaculture. *Nature* 591, 551–563. <https://doi.org/10.1038/s41586-021-03308-6>.
- Nilsen, A., 2019. *Production of Atlantic Salmon (Salmo salar) in Closed Confinement Systems (CCS) : Salmon Lice, Growth Rates, Mortality and Fish Welfare*. Norwegian University of Life Sciences, Ås.
- Oldham, T., Oppedal, F., Dempster, T., 2018. Cage size affects dissolved oxygen distribution in salmon aquaculture. *Aquacult. Environ. Interact.* 10, 149–156. <https://doi.org/10.3354/aei00263>.
- Park, S., Lee, J., Lee, C.-W., 2021. Design evaluation of a fish cage mooring system with different bridle line connections using model experiments and simulations. *Aquacult. Eng.* 94, 102177. <https://doi.org/10.1016/j.aquaeng.2021.102177>.
- Priour, D., 2013. In: *A Finite Element Method for Netting: Application to Fish Cages and Fishing Gear*, first ed. Springer Netherlands, Dordrecht. <https://doi.org/10.1007/978-94-007-6844-4>. 2013.
- Qu, X., Hu, F., Kumazawa, T., Takeuchi, Y., Dong, S., Shioda, D., Tokai, T., 2019. Deformation and drag force of model square fish cages in a uniform flow. *Ocean. Eng.* 171, 619–624. <https://doi.org/10.1016/j.oceaneng.2018.12.016>.
- Reite, K.-J., Fore, M., Aarsæther, K.G., Jensen, J., Rundtop, P., Kyllingstad, L.T., Endresen, P.C., Kristiansen, D., Johansen, V., Fredheim, A., 2014. Fhsm — time domain simulation of marine systems. In: Presented at the ASME 2014 33rd International Conference on Ocean, Offshore and Arctic Engineering. American Society of Mechanical Engineers Digital Collection, San Francisco, California, USA. <https://doi.org/10.1115/OMAE2014-23165>.
- Ruzzo, C., Muggiasca, S., Malara, G., Taruffi, F., Belloli, M., Collu, M., Li, L., Brizzi, G., Arena, F., 2021. Scaling strategies for multi-purpose floating structures physical modeling: state of art and new perspectives. *Appl. Ocean Res.* 108, 102487. <https://doi.org/10.1016/j.apor.2020.102487>.
- Schubel, J.R., Thompson, K., 2019. Farming the sea: the only way to meet humanity's future food needs. *GeoHealth* 3, 238–244. <https://doi.org/10.1029/2019GH000204>.
- Shainee, M., Ellingsen, H., Leira, B.J., Fredheim, A., 2013a. Design theory in offshore fish cage designing. *Aquaculture* 392 (395), 134–141. <https://doi.org/10.1016/j.aquaculture.2013.02.016>.
- Shainee, M., Leira, B.J., Ellingsen, H., Fredheim, A., 2013b. In: An Optimum Design Concept for Offshore Cage Culture. Presented at the ASME 2012 31st International Conference on Ocean, Offshore and Arctic Engineering. American Society of Mechanical Engineers Digital Collection, pp. 85–93. <https://doi.org/10.1115/OMAE2012-83601>.
- Shimizu, T., Takagi, T., Korte, H., Hiraishi, T., Yamamoto, K., 2007. Application of NaLA, a fishing net configuration and loading analysis system, to bottom gill nets. *Fish. Sci.* 73, 489–499. <https://doi.org/10.1111/j.1444-2906.2007.01361.x>.
- Sievers, M., Korsøen, Ø., Warren-Myers, F., Oppedal, F., Macaulay, G., Folkedal, O., Dempster, T., 2021. Submerged cage aquaculture of marine fish: a review of the biological challenges and opportunities. *Rev Aquacult raq* 12587. <https://doi.org/10.1111/raq.12587>.
- Standards Norway, 2009. *NS 9415 marine fish farms—requirements for design. In: Dimensioning, Production, Installation and Operation*.
- Skjong, S., Reite, K.-J., Aarsæther, K.G., 2021. Lumped, constrained cable modeling with explicit state-space formulation using an elastic version of Baumgarte stabilisation. *J. Offshore Mech. Arctic Eng.* 1–15. <https://doi.org/10.1115/1.4050422>.
- Su, B., Reite, K.-J., Fore, M., Aarsæther, K.G., Alver, M.O., Endresen, P.C., Kristiansen, D., Haugen, J., Caharjja, W., Tsarau, A., 2019. A multipurpose framework for modelling and simulation of marine aquaculture systems. In: Presented at the ASME 2019 38th International Conference on Ocean, Offshore and Arctic Engineering. American Society of Mechanical Engineers Digital Collection. <https://doi.org/10.1115/OMAE2019-95414>.
- Su, B., Tsarau, A., Endresen, P.C., Kristiansen, D., Lader, P.F., 2021. Numerical study of closed rigid fish cages in waves and comparison with experimental data. *Ocean. Eng.* 233, 109210. <https://doi.org/10.1016/j.oceaneng.2021.109210>.
- Suzuki, K., Takagi, T., Shimizu, T., Hiraishi, T., Yamamoto, K., Nashimoto, K., 2003. Validity and visualisation of a numerical model used to determine dynamic configurations of fishing nets. *Fish. Sci.* 69, 695–705. <https://doi.org/10.1046/j.1444-2906.2003.00676.x>.
- Takagi, T., Suzuki, K., Hiraishi, T., 2002. Modeling of net for calculation method of dynamic fishing net shape. *Fish. Sci.* 68, 1857–1860. <https://doi.org/10.2331/fishsci.68.sup2.1857>.
- Takagi, T., Miyata, S., Fusejima, I., Oshima, T., Uehara, T., Suzuki, K., Nomura, Y., Kanechiku, M., Torisawa, S., 2014. Effect of mesh size on sinking characteristics of purse seine net. *J. Fish. Eng.* 51, 11–19. <https://doi.org/10.18903/fisheng.51.1.11>.
- Tsukrov, I., Eroshkin, O., Fredriksson, D., Swift, M.R., Celikkol, B., 2003. Finite element modeling of net panels using a consistent net element. *Ocean. Eng.* 30, 251–270. [https://doi.org/10.1016/S0029-8018\(02\)00021-5](https://doi.org/10.1016/S0029-8018(02)00021-5).
- Wan, R., Guan, Q., Li, Z., Hu, F., Dong, S., You, X., 2020. Study on hydrodynamic performance of a set-net in current based on numerical simulation and physical model test. *Ocean. Eng.* 195, 106660. <https://doi.org/10.1016/j.oceaneng.2019.106660>.
- Wang, X., Wan, R., Zhao, F., Huang, L., Sun, P., Tang, Y., 2016. Comparative study of dynamics of gravity cages with different meshes in waves and current. In: Presented at the ASME 2016 35th International Conference on Ocean, Offshore and Arctic Engineering. American Society of Mechanical Engineers Digital Collection. <https://doi.org/10.1115/OMAE2016-54549>.
- Xu, Z., Qin, H., 2020. Fluid-structure interactions of cage based aquaculture: from structures to organisms. *Ocean. Eng.* 217, 107961. <https://doi.org/10.1016/j.oceaneng.2020.107961>.
- Zhao, Y.-P., Li, Y.-C., Dong, G.-H., Gui, F.-K., Teng, B., 2007a. A numerical study on dynamic properties of the gravity cage in combined wave-current flow. *Ocean. Eng.* 34, 2350–2363. <https://doi.org/10.1016/j.oceaneng.2007.05.003>.
- Zhao, Y.-P., Li, Y.-C., Dong, G.-H., Gui, F.-K., Teng, B., 2007b. Numerical simulation of the effects of structure size ratio and mesh type on three-dimensional deformation of

- the fishing-net gravity cage in current. *Aquacult. Eng.* 36, 285–301. <https://doi.org/10.1016/j.aquaeng.2007.01.003>.
- Zhao, Y.-P., Li, Y.-C., Gui, F.-K., Dong, G.-H., 2007c. Numerical simulation of the effects of weight system on the hydrodynamic behavior of 3-D net of gravity cage in current. *J. Hydrodyn.* 19, 442–452. [https://doi.org/10.1016/S1001-6058\(07\)60138-3](https://doi.org/10.1016/S1001-6058(07)60138-3).
- Zhao, Y.-P., Bi, C.-W., Chen, C.-P., Li, Y.-C., Dong, G.-H., 2015a. Experimental study on flow velocity and mooring loads for multiple net cages in steady current. *Aquacult. Eng.* 67, 24–31. <https://doi.org/10.1016/j.aquaeng.2015.05.005>.
- Zhao, Y.-P., Wang, X.-X., Decew, J., Tsukrov, I., Bai, X.-D., Bi, C.-W., 2015b. Comparative study of two approaches to model the offshore fish cages. *China Ocean Eng.* 29, 459–472. <https://doi.org/10.1007/s13344-015-0032-0>.